

Technical Report ISPIDA

Team 02 Technical Report to the 2025 EuRoC



Aerospace Team Graz (ASTG) Graz University of Technology

Graz, September 30, 2025

Contact:

Technical Lead:

l.ruprecht@astg.at

Organizational Lead:

g.kurzmann@astg.at

Abstract

ISPIDA is the fifth launch vehicle developed by ASTG and represents the team's most advanced rocket to date. It was designed to compete in the EuRoC SRAD 9000 m hybrid flight (H9) category. The overall length of ISPIDA is 4357 mm, with a diameter of 152.4 mm and a total liftoff mass of 47.0 kg.

The single-stage hybrid uses Hydroxyl Terminated Polybutadiene (HTPB) as solid fuel, N_2O as oxidizer, and N_2 as pressurizing gas. With a burn time of 9.5 s and a total impulse of 32.1 kNs, the propulsion system enables the vehicle to reach its target apogee of 9000 m.

A characteristic of ISPIDA is its actively controlled propulsion system. The fluid subsystem incorporates an electronically regulated pressurization valve (E-Reg), which provides a stable oxidizer tank pressure. The combustion chamber features a unique twisted finocyl geometry that enhances regression rate and combustion efficiency without the need for energetic additives.

The aerostructure is optimized for strength-to-weight efficiency, using CFRP and GFRP composites depending on RF-transparency requirements. An integrated air brake system provides active apogee targeting, while a dedicated Pitot-Static Probe enables real-time airspeed and altitude measurements to support guidance and telemetry.

The custom-developed flight computer integrates power management, avionics, and recovery electronics. It collects data from multiple barometers, Inertial Measurement Units (IMUs), sun sensors, and internal thrust measurements. Distributed CANary nodes provide robust data acquisition across subsystems.

The rocket's systems communicate through an SRAD telemetry system that employs a self-developed packet protocol across multiple data links, including wireless LoRa and both wired and wireless ground networks. The LoRa communication is made possible by a custom patch antenna system mounted on the outside of the rocket.

For recovery, ISPIDA employs a dual-deployment parachute system with full electrical and mechanical redundancy, ensuring reliable separation of the main vehicle and the guided nosecone at apogee. Integrated into the nosecone is BUBO, a guided landing vehicle. While the rocket descends under drogue and main parachutes, BUBO descends with a steerable parafoil below 450 m and, equipped with its own avionics stack and telemetry, autonomously navigates to a predefined landing zone.

The payload mission is provided by WüSpace, a partner student team. Their 1U CubeSat, "S²OUTH", is placed into the avionics section and supports live video transmission up to 200 km. This collaboration highlights the interdisciplinary and inter-university nature of the project.

The objectives of the ISPIDA project extend beyond the EuRoC competition. Besides reaching the target apogee of 9000 m and demonstrating autonomous guided recovery, the project aims to mature ASTG's hybrid propulsion expertise as a stepping stone towards future liquid engines, while ensuring sustainable knowledge transfer to younger members. By combining innovative propulsion technologies, a unique guided recovery system, and a collaborative payload mission, ISPIDA serves as both a high-impact EuRoC competitor and a long-term educational platform for advancing student rocketry at Graz University of Technology (TU Graz).



Contents

1	Intr	roduction 1			
	1.1	Partn	ers and Supporters	2	
	1.2	Projec	ct Goals and Mission Objectives	2	
_					
2		nch Ve	hicle System Architecture		
	2.1	Syster	m Overview		
	2.2	-	llsion Subsystem		
		2.2.1	Fluid System		
	2.2	2.2.3	Testing		
	2.3		tructure Subsystem		
		2.3.1	Structure		
		2.3.2	Aerodynamics		
	0.4	2.3.3	Pitot-Static System		
	2.4		rery Subsystem		
		2.4.1	Overview Recovery Section		
		2.4.2	Redundancy		
		2.4.3	Chargecups		
		2.4.4	First Deployment		
		2.4.5	Second Deployment		
		2.4.6	Parachutes		
		2.4.7	Parachute Lines and Connections		
		2.4.8	Recovery System Tests		
	2.5		d Nosecone		
		2.5.1	Nosecone-Assembly		
		2.5.2	Parachutes and lines		
	2.6	Flight	Computer Subsystem		
		2.6.1	Power System		
		2.6.2	Avionics Stack		
		2.6.3	Avionics Stack PCBs	2	
		2.6.4	Supporting PCBs	1	
		2.6.5	Recovery Electronics	5	
		2.6.6	Flight Computer Software	3	
	2.7	Telem	etry Subsystem)	
		2.7.1	Patch Antenna System)	
		2.7.2	Printed Circuit Boards (PCBs))	
		2.7.3	Nosecone Telemetry System	L	
		2.7.4	Firmware	L	
		2.7.5	Teltalk Communication Protocol	L	
	2.8	Pavlo	ad Subsystem	3	
		2.8.1	Project Description "S ² OUTH"	3	
		2.8.2	System Architecture		
		2.8.3	Telemetry Link		
		2.8.4	Live Video Stream		
		2.8.5	Support Systems		
		2.0.0		•	
3	Miss	sion Co	oncept of Operations Overview 44	1	
	3.1	Armir	ng of the System	1	
	3.2		ng and Pressurizing	1	
	3.3		nal Flight	5	
		3.3.1	Boost Phase		
		3.3.2	Coast Phase		
		3.3.3	Drogue Descent Phase		
		3.3.4	Main Descent Phase		

	3.4 3.5 3.6	Thrust Curves	46 46 47
4	Con	clusions and Outlook	48
Lis	st of I	Figures	vii
Lis	st of T	Tables	ix
Αc	rony	ms	X
GI	ossar	ry >	ciii
Re	ferer	nces	χv
Αŗ	pend	dix A: System Data	49
Αŗ			53
-	B.1	Filling Station	53
		B.1.1 Fluid Architecture	53
			54
			54
	B.2		54
	D.Z		5 5
			55
			56
			56
	B.3		57
		B.3.1 Mission Control Hardware	57
		B.3.2 Control Panel and Visualization	58
			59
Αŗ	pend	dix C: Detailed Test Reports	60
•	C.1	Testing List	60
	C.2		64
	C.3		66
		0 1	67
	C.4 C.5		71
			75
	C.7		82
	C.8		95
	C.9	Second Deployment Concept Test	99
	C.10	Second Deployment Functionality Test	.01
	C.11	Second Deployment Vibration Test	13
		RTA Windtunnel Test	
		RTA Windtunnel Test	
		Main Parachute Pull-Out Test	
		SPATZ Flight	
		Nosecone Separation Test	
		Nosecone Separation Overload	
		Deployment Flight Computer Actuation	.59
	C.19	Recovery Pressure Sensor Test	65
	C.20	Recovery Pre-Assembly Test	66
		Vacuumchamber NC Ejection	68
		Drone Verification Test	
		Initial Parafoil Test	
		Parafoil Deployment Test	
		Tension Scale Test	
	L. /.b	All Up Vertical	200

C.27 Launch Dry Run	 			208
C.28 Cold-Flow 1: horizontal				
C.29 Hot-Fire 1: horizontal				
C.30 Hot-Fire 2: horizontal				
C.31 Hot-Fire 3: horizontal				
C.32 Hot-Fire 4: horizontal				
C.33 Hot-Fire 5: vertical				
C.34 Hot-Fire 6: vertical	 			262
C.35 Ignitor Test	 			269
C.36 E-Reg Tests	 			277
C.37 Umbilical Test				
C.38 Combustion Chamber Pressure Test				
C.39 Oxidizer Tank Pressure Test				
C.40 Tube Bending Test				
C.41 Air Brake Actuation Test				
C.42 Air Brake Shaker Test				
C.43 Rail Fit Test				
C.44 Adhesive Heating Test	 			299
C.45 Fin Alignment Test				
C.46 Holddown Static Load Deployment Test				
C.47 Holddown Dynamic Load Deployment Test	 			309
C.48 Holddown Hardpoint Test	 			312
C.49 Holddown Hardpoint Test				
C.50 Electrical Umbilical				
C.51 Vibration Test				
C.52 Long Duration Runtime Test				
C.53 CATS Test				
C.54 Range Test				
C.55 Antenna Specification Test				
C.56 Telemetry Data Rate Test	 •	•		344
Annandiy D. Hanayd Analysis Danayt				246
Appendix D: Hazard Analysis Report D.1 Hazardous Substances				346
D.1 Hazardous Substances	 •	• •		346
Appendix E: Risk Assessment				350
E.1 FMECA Explanation	 •	• •		350
E.1.1 Risk Calculation Matrix	 	• •		351
Annandiy Fr. Compliance Matrix				204
Appendix F: Compliance Matrix				384
				400
Annendix G: Checklists				
Appendix G: Checklists G.1. Checklists Checklist				
G.1 Checklists Checklist				
G.1 Checklists Checklist	 			100
G.1 Checklists Checklist	 			
G.1 Checklists Checklist	 		 	408
G.1 Checklists Checklist	 	· ·	· ·	408 410
G.1 Checklists Checklist	 	· ·	· ·	408 410
G.1 Checklists Checklist	 	 	 	408 410 413
G.1 Checklists Checklist				408 410 413 415
G.1 Checklists Checklist			· · · · · · · · · · · · · · · · · · ·	408 410 413 415 418
G.1 Checklists Checklist G.2 Launch Procedure G.3 General Abort G.4 Propulsion GSE Setup G.5 Combustion Chamber Assembly G.6 Fuelgrain Casting G.7 Ignitor Casting G.8 Propulsion Stack Integration G.9 Pre-Assembly Recovery Section				408 410 413 415 418 420
G.1 Checklists Checklist G.2 Launch Procedure G.3 General Abort G.4 Propulsion GSE Setup G.5 Combustion Chamber Assembly G.6 Fuelgrain Casting G.7 Ignitor Casting G.8 Propulsion Stack Integration G.9 Pre-Assembly Recovery Section G.10 Final Assembly Recovery Section				408 410 413 415 418 420 426
G.1 Checklists Checklist G.2 Launch Procedure G.3 General Abort G.4 Propulsion GSE Setup G.5 Combustion Chamber Assembly G.6 Fuelgrain Casting G.7 Ignitor Casting G.8 Propulsion Stack Integration G.9 Pre-Assembly Recovery Section G.10 Final Assembly Recovery Section G.11 Recovery First Deployment Assembly			· · · · · · · · · · · · · · · · · · ·	408 410 413 415 418 420 426 430
G.1 Checklists Checklist G.2 Launch Procedure G.3 General Abort G.4 Propulsion GSE Setup G.5 Combustion Chamber Assembly G.6 Fuelgrain Casting G.7 Ignitor Casting G.8 Propulsion Stack Integration G.9 Pre-Assembly Recovery Section G.10 Final Assembly Recovery Section G.11 Recovery First Deployment Assembly G.12 Recovery Second Deployment Assembly				408 410 413 415 418 420 426 430 432
G.1 Checklists Checklist G.2 Launch Procedure G.3 General Abort G.4 Propulsion GSE Setup G.5 Combustion Chamber Assembly G.6 Fuelgrain Casting G.7 Ignitor Casting G.8 Propulsion Stack Integration G.9 Pre-Assembly Recovery Section G.10 Final Assembly Recovery Section G.11 Recovery First Deployment Assembly G.12 Recovery Second Deployment Assembly G.13 Recovery Chargecup Preparation				408 410 413 415 418 420 426 430 432 434
G.1 Checklists Checklist G.2 Launch Procedure G.3 General Abort G.4 Propulsion GSE Setup G.5 Combustion Chamber Assembly G.6 Fuelgrain Casting G.7 Ignitor Casting G.8 Propulsion Stack Integration G.9 Pre-Assembly Recovery Section G.10 Final Assembly Recovery Section G.11 Recovery First Deployment Assembly G.12 Recovery Second Deployment Assembly G.13 Recovery Chargecup Preparation G.14 Main Parachute Folding				408 410 413 415 418 420 426 430 432 434 437
G.1 Checklists Checklist G.2 Launch Procedure G.3 General Abort G.4 Propulsion GSE Setup G.5 Combustion Chamber Assembly G.6 Fuelgrain Casting G.7 Ignitor Casting G.8 Propulsion Stack Integration G.9 Pre-Assembly Recovery Section G.10 Final Assembly Recovery Section G.11 Recovery First Deployment Assembly G.12 Recovery Second Deployment Assembly G.13 Recovery Chargecup Preparation G.14 Main Parachute Folding G.15 Drogue Folding				408 410 413 415 418 420 426 430 432 434 437 441
G.1 Checklists Checklist G.2 Launch Procedure G.3 General Abort G.4 Propulsion GSE Setup G.5 Combustion Chamber Assembly G.6 Fuelgrain Casting G.7 Ignitor Casting G.8 Propulsion Stack Integration G.9 Pre-Assembly Recovery Section G.10 Final Assembly Recovery Section G.11 Recovery First Deployment Assembly G.12 Recovery Second Deployment Assembly G.13 Recovery Chargecup Preparation G.14 Main Parachute Folding G.15 Drogue Folding G.16 Recovery Disassembly				408 410 413 415 418 420 426 430 432 434 437 441 443
G.1 Checklists Checklist G.2 Launch Procedure G.3 General Abort G.4 Propulsion GSE Setup G.5 Combustion Chamber Assembly G.6 Fuelgrain Casting G.7 Ignitor Casting G.8 Propulsion Stack Integration G.9 Pre-Assembly Recovery Section G.10 Final Assembly Recovery Section G.11 Recovery First Deployment Assembly G.12 Recovery Second Deployment Assembly G.13 Recovery Chargecup Preparation G.14 Main Parachute Folding G.15 Drogue Folding				408 410 413 415 418 420 430 432 434 437 441 443 450

G.19 PSP Stack Assembly	454
G.20 Flight Computer Assembly	
G.21 Flight Computer Pre-Launch	
G.22 Flight Readiness	459
G.23 Filling Station Electronics Assembly	460
G.24 Nosecone Pre-Assembly	462
G.25 Nosecone Final Integration	466
G.26 Parafoil Deployment	469
G.27 Parafoil Folding	471
G.28 Steering Mechanism	474
G.29 ParaCAM	476
G.30 FlightCAM	477
G.31 Nosecone Disassembly	478
G.32 Telemetry Mission Control Setup	479
G.33 Telemetry GSE Setup	
G.34 Telemetry Pre-Assembly	482
A Property Letters and the	40.
	485
H.1 3km Flight Simulation	
H.2 9km Flight Simulation without BUBO	
H.3 9km Flight Simulation with BUBO	535
Appendix I: Engineering Drawings	551
Appendix J: PCB Schematics	618
Appendix J. FCB Schematics	010
Appendix K: Detailed Structural and Mechanical Calculations	739
Appendix L: Further System Details	938
L.1 Recovery Line Management	938
L.2 Nosecone Line Management	
L.3 Datasheets	
L.3.1 Recovery Datasheets	
L.3.2 Propulsion Datasheets	
L.3.3 Telemetry Datasheets	



1 Introduction

ASTG was founded in 2019 by students of TU Graz. Since then, it has grown to around 90 members from 15 different fields of study. All members are united by the passion for space and rocketry, but also by the desire to create their own projects and bring the theory taught in university into reality.

Since its debut at European Rocketry Challenge (EuRoC) 2021, a major focus of ASTG has been the design and development of competitive rockets for future EuRoC editions. The progression of these projects is shown in Figure 1.1, from the solid-propelled AVES and AVES II to the hybrid-propelled HALCYON and ALCEDO. The most recent vehicle, ISPIDA, is the team's fifth competition rocket and the third powered by a hybrid engine.

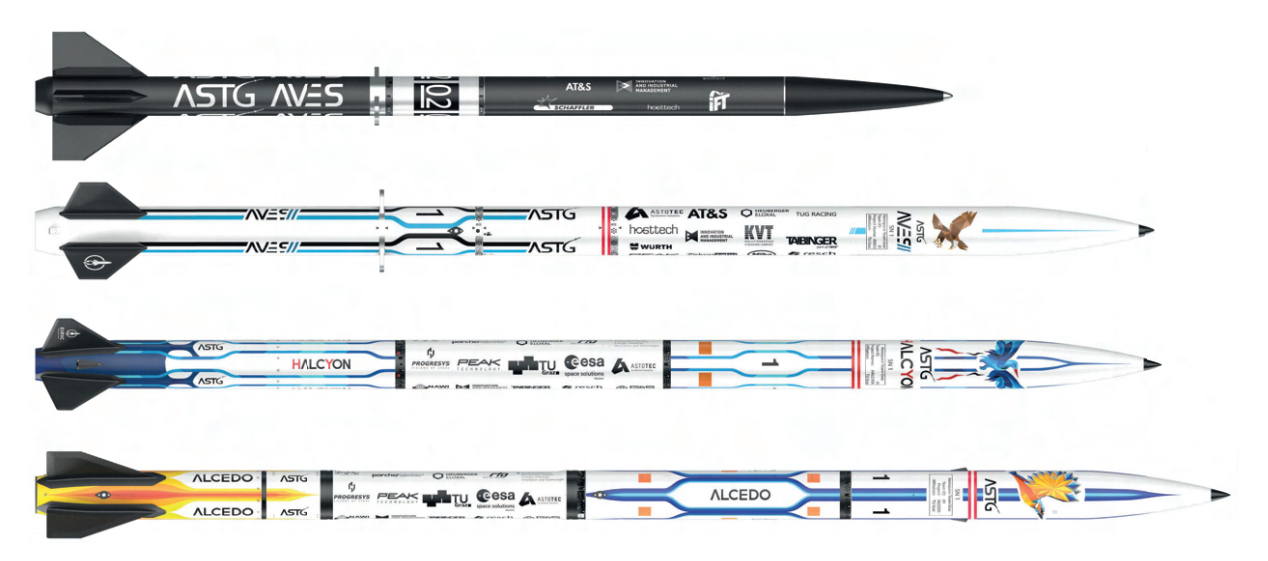


Figure 1.1: Progression of all competition rockets developed by ASTG from 2021 to present.

ASTG brings together students from different academic fields, study levels, and age groups. Despite the challenges of recruiting from traditionally male-dominated disciplines, about one-fifth of the team are women. This range of backgrounds brings together a diverse set of perspectives, which strengthens the team's ability to tackle complex projects. Figure 1.2 illustrates the demographic composition of the team.

ASTG structures its work into project teams, each divided into modules responsible for specific subsystems. For ISPIDA, the Project Lead coordinates time, resources, interfaces, risks, and documentation together with the Module Leaders and System Engineers. Five modules cover the main technical areas: the Aerostructure Module (AST) develops the airframe and structural components; the Flight Computer Module (FLI) advances software and hardware for the Student Researched and Developed (SRAD) flight computer, including sensor data, valve actuation, and Ground Support Equipment (GSE) control; the Telemetry Module (TEL) ensures reliable data links and position tracking; the Propulsion Module (PRO) designs the propulsion system, ground support, and Hot-Fire testing facilities; and the Recovery Module (REC) develops the dual-deployment recovery system and its test setups.

In addition to rocket development, ASTG took on a second challenge by joining the Rocket Experiment for University Students (REXUS) program. Accepted in 2024, the Auroral Polarization EXplorer (APEX) project aims to measure the polarization of the aurora borealis and is scheduled to launch from Kiruna in March 2026.

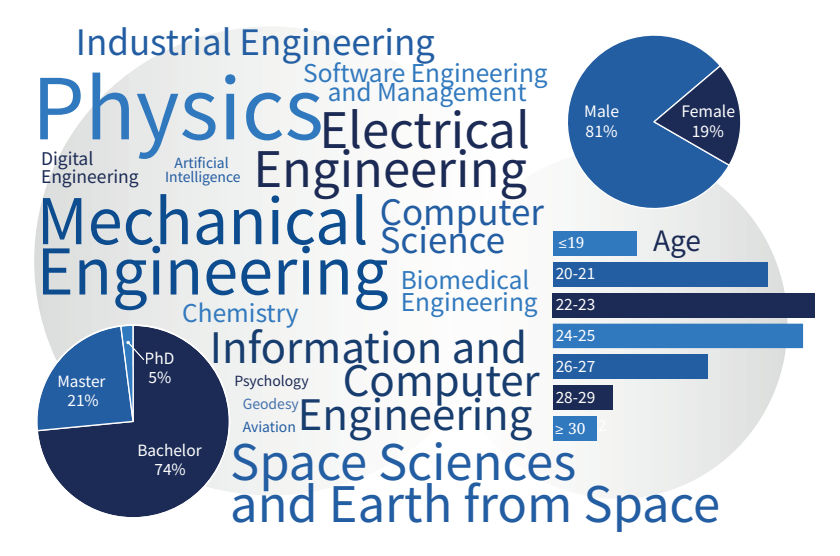


Figure 1.2: Overview of the team demographics showing study levels, gender distribution, the fields of studies, and age distribution.

1.1 Partners and Supporters

Despite the hard work and effort put in by all the motivated team members, realizing such a demanding project requires sponsorship and collaboration with numerous partners. The overall support is divided into contributions from educational institutions, public funds, and businesses in various forms, such as monetary donations, the supply of tools and materials, the provision of manufacturing capabilities, software licenses, testing facilities, and the sharing of expertise and advice. Sponsors from this year include TU Graz, Austrian Research Promotion Agency (FFG), Institute of Production Engineering (IFT), Institute of Innovation and Industrial Management (IIM), Astotec Pyrotechnic Solutions GmbH, Peak Technology GmbH, Resch GmbH and over sixty more.

Furthermore, for project ISPIDA, ASTG collaborated with WüSpace, who provided the 1U CubeSat "S²OUTH". WüSpace uses ISPIDA as a testing platform for their electronics before future higheraltitude missions.

1.2 Project Goals and Mission Objectives

The goals for project ISPIDA were defined as:

- Improve the performance and reliability of subsystems by implementing design optimizations and additional testing.
- Transfer knowledge to future team members by creating a high-quality and comprehensive technical documentation.
- Reach the top five at EuRoC'25.

The mission objectives for ISPIDA were defined as:

- Reach an altitude of 9000 m.
- Land the nosecone at a designated landing site using a guided parafoil.
- Transport the 1U CubeSat, "S²OUTH" (WüSpace), to 9000 m, where it provides live video transmission.



2 Launch Vehicle System Architecture

2.1 System Overview

The ISPIDA system architecture integrates multiple subsystems into a cohesive hybrid rocket capable of reaching an altitude of 9000 m. As shown in Figure 2.1, ISPIDA consists of six distinct sections. The nosecone houses BUBO, the guided landing vehicle. The next section is the recovery section, which contains the parachutes and their deployment mechanisms. The avionics section houses the SRAD flight computer, the CATS Vega, the CubeSat, and the COPV. It is connected to the oxidizer tank, which connects to the combustion chamber through the valve bay structure and the air brake.

The propulsion system features a combustion chamber, oxidizer tank with active pressure regulation (E-Reg), and a COPV for pressurant storage. Dual-redundant recovery systems deploy drogue parachutes and main parachutes through separate deployment charges (FD/SD). Radax connectors join major airframe sections while four fins provide aerodynamic stability.

The BUBO landing craft contains its flight computer, telemetry, and steerable parafoil system. Avionics include the main flight computer, CATS Vega, and distributed CANary modules for data acquisition. Two identical telemetry systems communicate with both systems, using either internal or patch antennas, depending on the RF transparency of the hull.

Ground support equipment comprises mission control interfaces, telemetry receivers, and the filling station with dedicated umbilicals for oxidizer and pressurant. The system incorporates several innovative design features that distinguish it from other hybrid rockets.

ISPIDA's most unique features include:

- Pitot-Static-Probe (PSP) for real-time airspeed and altitude measurement
- · BUBO guided landing system
- Recovery system with compact pressure chamber for reliable deployment
- E-Reg active pressure regulation system
- Twisted finocyl HTPB fuel grain for enhanced burn characteristics

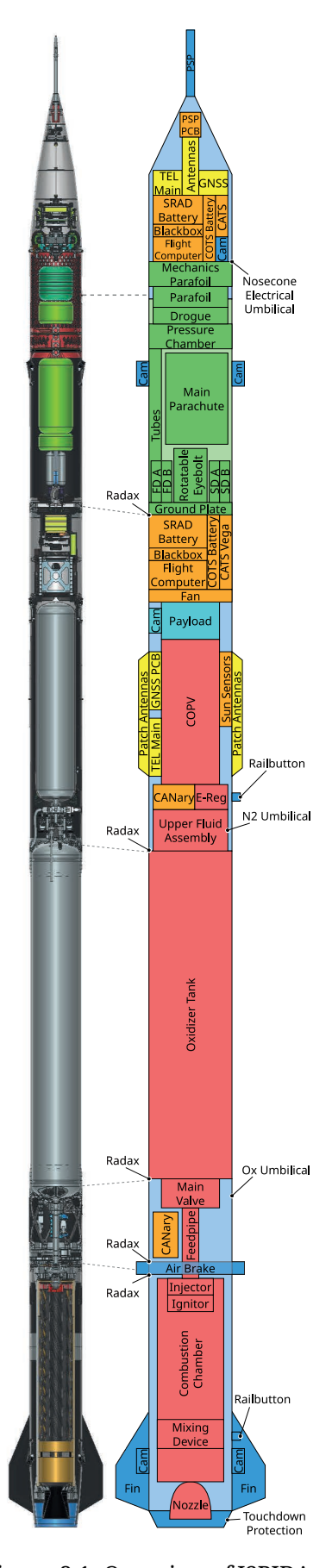


Figure 2.1: Overview of ISPIDA.



2.2 Propulsion Subsystem

The hybrid engine operates using nitrous oxide (N_2O) as the oxidizer, HTPB as the fuel and nitrogen (N_2) for pressurization. The mission objective is to achieve the full target apogee of 9 km. The engine concept is based on the predecessor and is systematically improved, with developments not only focused on meeting the current mission requirements but also aligned with the long-term goal of transitioning towards a liquid propulsion system.

The propulsion stack, depicted in Figure 2.2, has two main compartments: the fluid system and the combustion chamber. The fluid system primarily consists of a Composite overwrapped pressure vessel (COPV) and the oxidizer tank. Key components of the fluid system include:

- an actively controlled pressurization valve, which regulates the pressure in the oxidizer tank during the burn;
- two vent valves, one of which is actively controlled, this configuration allows for selecting either a 3 km or 9 km apogee, depending on the conditions such as weather and wind, with the rocket already on the launch pad;
- a cavitating venturi in the feed pipe, which regulates the oxidizer mass flow rate.

A dedicated cable duct routes all necessary wiring through the oxidizer tank downwards without requiring external mounting or modifications to the tank structure. The air brake is positioned between the oxidizer tank and the combustion chamber to shift the center of pressure as far aft as possible, contributing to aerodynamic stability.

Inside the combustion chamber, a swirl injector ensures atomization of the oxidizer. The HTPB fuel grain features a twisted finocyl geometry with integrated side ports and a mixing device, enabling highly efficient combustion and high thrust output.

Table 2.1: Engine characteristics.

S		
Characteristic	Value	Unit
Length	2.69	m
Pressurant Tank Pressure	300	bar
Oxidizer Tank Pressure	43	bar
Combustion Pressure	30	bar
Total Impulse	32.1	kNs
Burn Time	9.5	S
Oxidizer Mass	13.5	kg
Fuel Mass	2.5	kg
Empty Mass	14.9	kg



Figure 2.2: The propulsion stack.



2.2.1 Fluid System

Starting from the top a COPV, with a volume of $4.3\,L$, is used to store N_2 gas at $300\,bar$. The high pressure gas is used to pressurize the oxidizer tank instead of using only the ullage gases pressure for pressurization. This approach ensures faster launch readiness as well as a more constant pressure in the oxidizer tank and also allows for a lower temperature of -20 °C, to ensure more dense oxidizer storage.

In the upper fluid system there are two sensors, recording pressure and temperature of the N_2 tank, as well as two pressure sensors in the oxidizer tank for redundancy. These sensors are used to collect data, display the system status, and regulate the E-Reg valve. The E-Reg controls the pressurization of the oxidizer tank to keep a pressure of 43 bar. The Quick Disconnect (QD) supplies N_2 to the tank during the fueling procedure. It can also function as a pressure relief valve. A burst disc serves as safety feature which releases the pressure in the oxidizer tank in case of a critical overpressure situation.

The actively controlled upper vent valve is connected to a dip tube which reaches into the oxidizer tank. It enables the verification of a completed fueling procedure through observation of liquid venting. It can be used to ascertain an oxidizer mass of 13.5 kg in the oxidizer tank. The oxidizer tank also houses a cable duct which facilitates cable management inside the tank without the need for external channels. The counterpart of the upper vent valve is the lower vent valve which enables fueling for a 3 km instead of 9 km apogee. A dip tube is attached to the solenoid vent valve and it can be opened to vent all but 5.8 kg of oxidizer.

The oxidizer tank is connected to the combustion chamber via the valvebay structure and the air brake. The feed pipe, which passes through the valvebay as well as the air brake, allows the oxidizer to flow to the combustion chamber. The flow of oxidizer is managed in a first step by the main valve. A cavitating venturi, integrated into the feed pipe, restricts the mass flow. Additional to the lower vent valve a manual release valve is available to enable a manual detanking of oxidizer. This acts as an additional safety measure. The temperature sensor is used to monitor the temperature of the liquid phase of the oxidizer. The lower QD is responsible for fueling the liquid oxidizer N_2O into the tank.

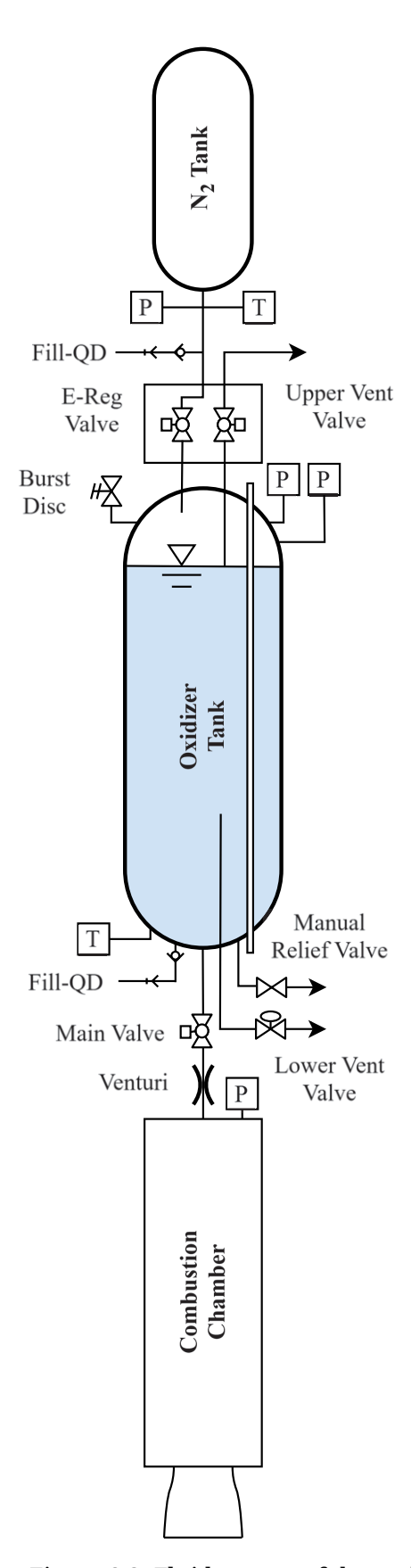


Figure 2.3: Fluid system of the rocket.



Upper Fluid System

The core element of the upper fluid system is the pressure tank connector, which is directly connected to a custom-designed valve body. This valve body houses both the pressurizing valve and venting valve. Located on either side of the pressure tank connector are several key components: a check valve with QD port for nitrogen N_2 filling, a 300 bar pressure sensor for monitoring the N_2 pressure, a thermocouple for the N_2 temperature, and a port for venting during oxidizer filling. The top port of the connector allows the COPV to be directly screwed on.

Mounted to the left and right of the valve body are RC servos, which actuate the pressurizing and venting valves through a geared mechanism. The angular position of the valves is monitored using custom designed valve angle sensors. At the rear of the assembly, a CANary is mounted to manage signal processing and control functions. The entire upper fluid assembly is structurally attached to the oxidizer tank using four supporting rods.

In the middle of the supporting rods, two fluid lines enter the oxidizer tank. On the pressurizing valve side, the line ends in a pressurizing deflector with radial holes designed to mitigate a direct blast of N_2 into the oxidizer. On the vent valve side, the line reaches the expected liquid level of the oxidizer, allowing visual confirmation that oxidizer loading is complete when liquid venting occurs.

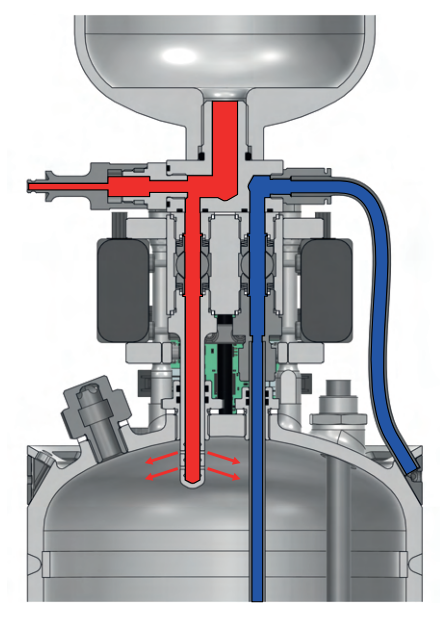


Figure 2.4: Red: pressurization path; Blue: oxidizer venting.

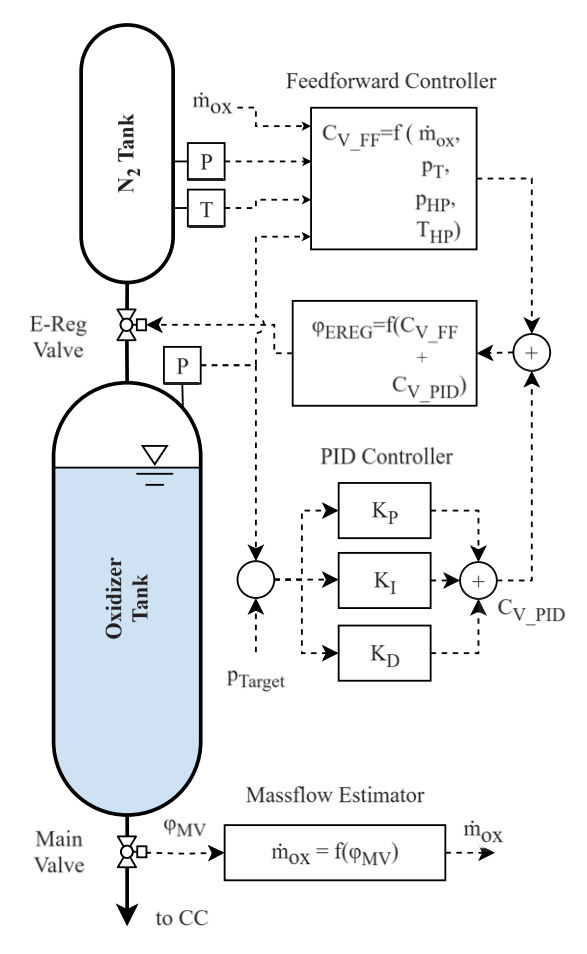


Figure 2.5: E-Reg controller overview.

Pressurizing System

For the pressurizing system, an actively controlled 1/4" ball valve (E-Reg) instead of a mechanical pressure regulator was chosen. This yields a light, compact and versatile system without the drawbacks of mechanical regulators with lock-up and supply-pressure effects.

The controller is a combination of a feedforward and Proportional Integral Differential (PID) controller, as depicted in Figure 2.5. The feedforward control takes the thermodynamic state of the pressurant tank and the oxidizer mass flow and calculates with assumed isenthalpic expansion the required flow coefficient C_v . The PID controller is similarly used to compensate startup transients and inaccuracies in the system models. Afterwards, both outputs are added and converted into a control output with the characteristic valve curve.

As the E-Reg valve is the only component that separates the high pressure pressurizing system from the oxidizer tank, an extensive safety controller was implemented, which checks for sensor failures and pressure values outside of safe limits. In the pre-launch state the controller will abort at any anomaly, while in the launched state, which is defined by the main valve opening, the software will try to keep E-Reg operational as long as possible by disabling certain parts of the controller.

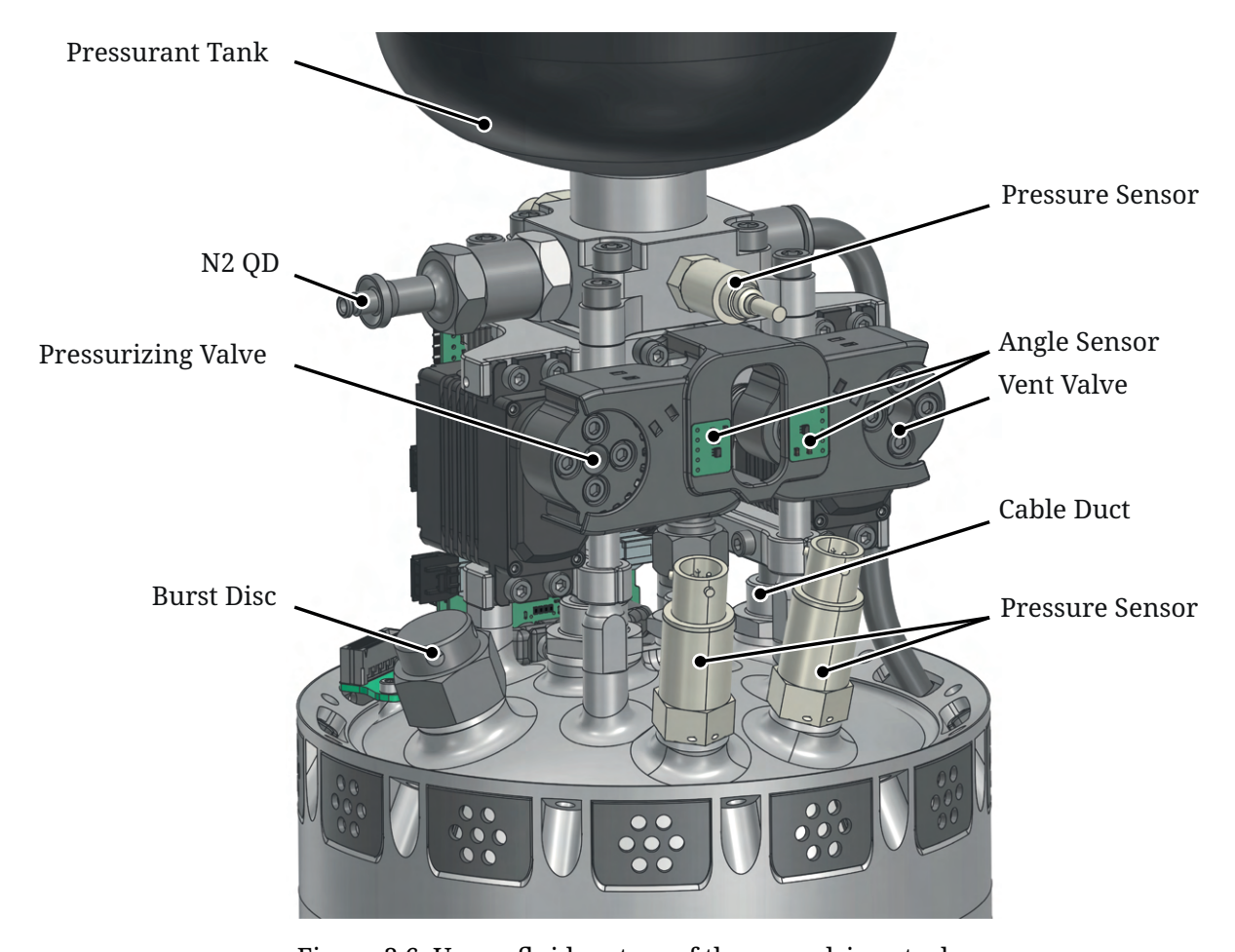


Figure 2.6: Upper fluid system of the propulsion stack.

Oxidizer Tank

The oxidizer tank holds the liquid nitrous oxide N_2O used as oxidizer in the engine. It has an internal volume of 15.6 L and holds 13.5 kg of N_2O in the nominal flight configuration. The tank is manufactured from aluminum EN-AW 6082-T6 and consists of a central cylindrical tube with the upper and lower bulkheads welded on. To prevent vortex formation and the resulting risk of ingesting gaseous oxidizer into the engine, two perforated plates are welded into the lower bulkhead above the outlet. The design pressure of the tank is 112 bar, with a maximum operating pressure of 56 bar.

The general design philosophy was carried over from previous flight tanks and consists of two main aspects: Firstly, making the tank a structural component of the rocket. Secondly, minimizing the fluid system plumbing through a fully integrated construction. The first aspect is achieved by having the structural mounting points integrated into the tank bulkheads. For the second aspect, all fluid system components are directly mounted to their dedicated ports in the bulkheads of the tank.

The lower bulkhead features a female 6-point Radax connection interfacing with the valve bay structure and holds the feed pipe and main valve for supplying the oxidizer to the engine. It also features connection ports for the oxidizer QD, manual relief valve, lower vent valve, and a thermocouple. The upper bulkhead is connected to the midsection shell through a female 12-point Radax connection. It also features mounting points for the upper fluid assembly and connection ports for the upper vent valve and dip tube, N_2 pressurization line, burst disc, and two pressure sensors. Both bulkheads also feature a connection for a tube leading through the entirety of the tank, acting as a cable duct and eliminating the need for an external one.



Main Valve

The main valve is a Commercial-off-the-shelf (COTS), three-piece 3/4" ball valve. The flanges of the valve are fully integrated into the system architecture, resulting in significant reductions in both overall weight and spatial requirements. The upper flange is directly embedded into the aluminum bulkhead of the oxidizer tank, while the lower flange is seamlessly integrated into the feed pipe that connects the valve to the combustion chamber. Compared to conventional configurations utilizing separate fittings and piping, this integrated design achieves a weight reduction of over 50 %.

Valve actuation is performed by a servo motor operating through a four-bar linkage mechanism. This linkage provides a variable transmission ratio, with the highest mechanical advantage occurring at the end positions. This characteristic is particularly beneficial for overcoming the initial breakaway torque during valve operation. The valve's position is continuously monitored by a custom designed valve angle sensor that is directly coupled to the shaft of the ball valve, ensuring precise feedback.

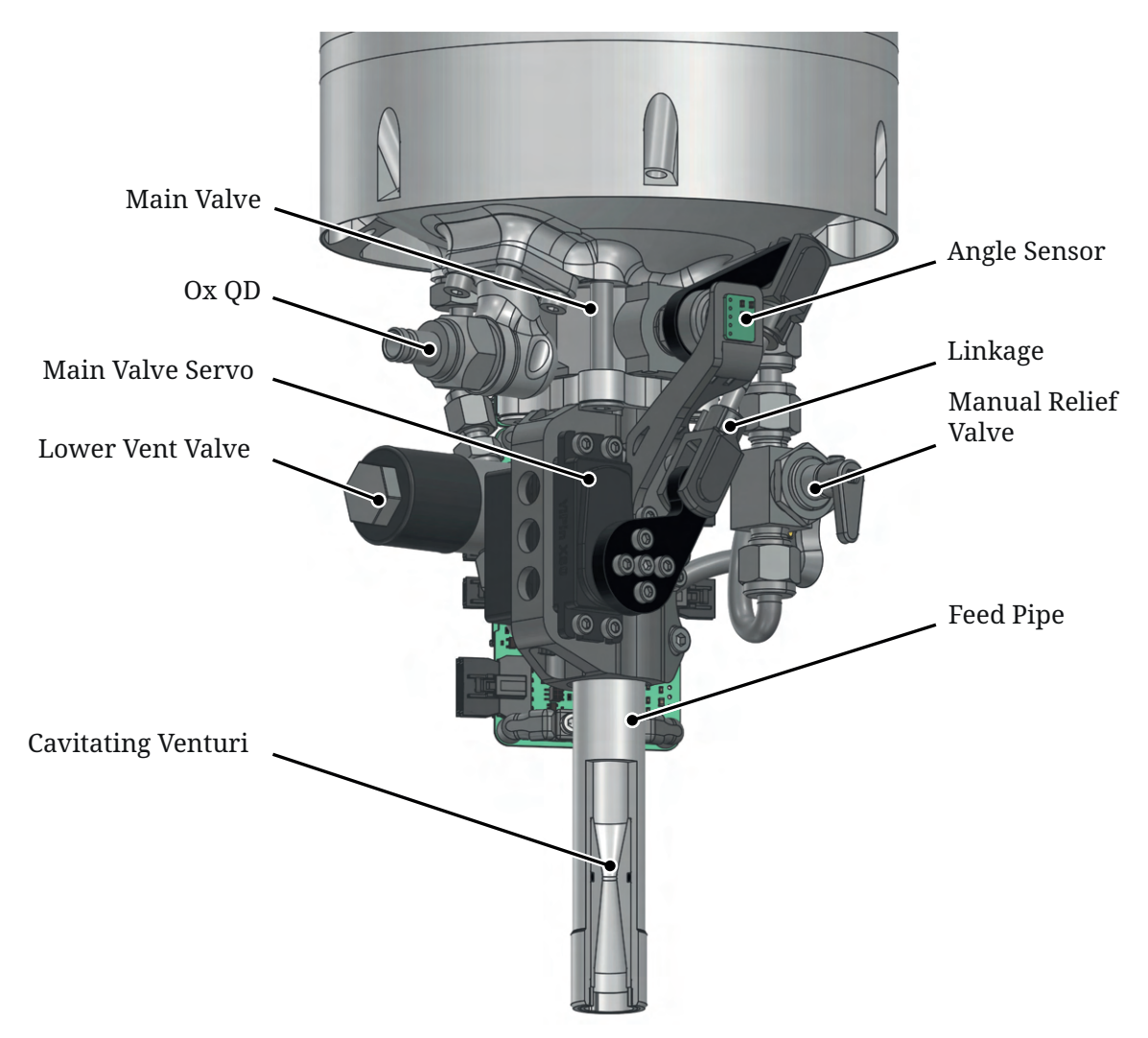


Figure 2.7: The lower bulkhead and the lower fluid assembly with the main valve and the feed pipe.

Cavitating Venturi

A cavitating venturi is installed in the oxidizer feed pipe between the oxidizer tank and the combustion chamber, serving as a passive flow regulation device. The component has an internal





diameter of 5.35 mm and was manufactured using resin stereo lithography 3d-printing. The design promotes controlled cavitation at the throat, ensuring a stable and repeatable mass flow rate once the upstream pressure exceeds the cavitation threshold. This behavior decouples the flow rate from moderate upstream pressure variations, providing a reliable oxidizer supply during combustion. The integration of the cavitating venturi is crucial for maintaining a consistent O/F ratio throughout the burn, thereby improving combustion stability, efficiency, and overall engine performance.

2.2.2 Combustion Chamber

The outermost layer of the combustion chamber is a cylindrical aluminum EN AW 6082-T6 casing. The tube is anodized to increase its surface hardness, thereby improving its durability against wear and scratches. Both ends are threaded to facilitate assembly and feature a smooth cylindrical face further inwards for sealing the combustion chamber with an O-ring.

The combustion chamber is closed off at the top by the bulkhead, an aluminum disc which acts as an interface between the combustion chamber and the injector as well as the injector cover. Additionally, a pressure needle allows a pressure sensor to be connected to the combustion chamber.

The injector cover features an O-ring groove on the outside to seal the interface with the bulkhead and two more on the top where the feed pipe is inserted. It features a conical transition to the larger injector diameter. When the injector cover is screwed onto the bulkhead, a small gap remains between them. This way, the injector cover presses tightly against the injector and holds it in place axially.

At the other end, the combustion chamber is enclosed by the graphite nozzle, a Laval nozzle with a converging and a diverging section. The nozzle is secured by the fuel grain insulation and a nozzle holder. The holder is kept in place against the combustion chamber pressure by a threaded retainer ring. The conical interface between nozzle and nozzle holder in combination with graphite paste seals the combustion chamber at the lower end. Additionally an O-ring seals the interface between nozzle holder and tube.

The inside of the casing is lined with the fuel grain insulation, which is tightly fit into the casing and firmly kept in place by screwing on the retainers onto both ends. The retainer also features eight screw holes to connect the combustion chamber to the air brake structure via an aluminum thrust plate, which is further detailed in Section 2.2.2.

The mixing device is positioned between the fuel grain and the nozzle in the post-combustion chamber, one-third of the way down from the fuel grain, and is secured in place by an additional layer of insulation. The purpose of the mixing device is to create turbulence in the combustion gases, thereby enhancing the mixing of N_2O and fuel. This improved mixing directly contributes to increased combustion efficiency, as documented by [1] and confirmed by the test campaign results.

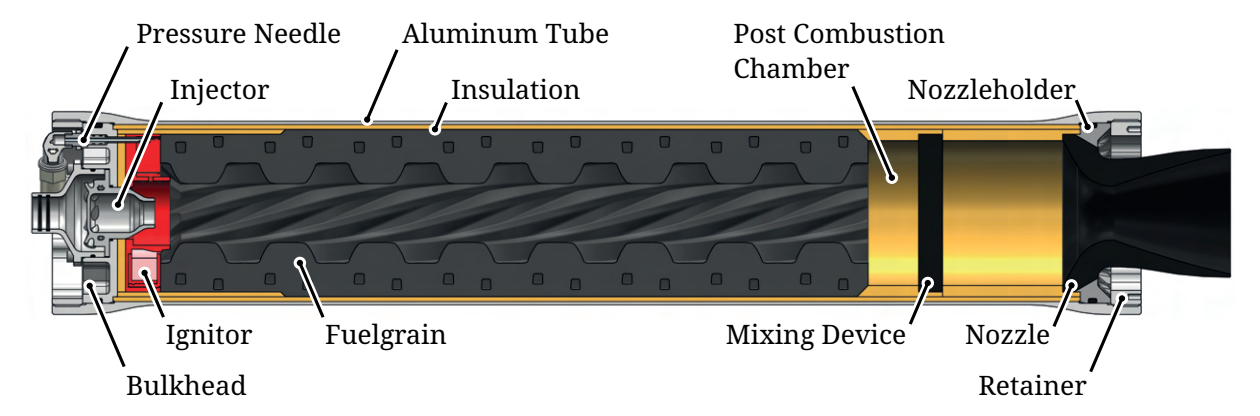


Figure 2.8: Shown is the combustion chamber assembly with its main components.



Thrust Plate

The thrust plate serves as a load-bearing interface between the combustion chamber and the air brake, transferring axial forces, primarily thrust and shock loads. To enable inflight measurement of these forces, four Wheatstone bridge circuits are integrated into the thrust plate. Each bridge consists of four strain gauges arranged to compensate for thermal effects, ensuring accurate load measurements despite temperature variations during engine operation. This setup allows for real-time acquisition of thrust data during flight, providing valuable input for performance analysis. For calibration purposes, the thrust plate was installed in series with load cells during the Hot-Fire test campaign.



Figure 2.9: Thrust Plate with strain gauges.

Injector

The ISPIDA injector system utilizes a single-element swirl injector to introduce and atomize the oxidizer within the combustion chamber, ensuring an optimal O/F ratio and efficient combustion. The oxidizer enters tangentially into a swirl chamber, creating a rotating flow that forms a thin liquid sheet. This sheet disintegrates into a conical spray upon exiting the nozzle, enhancing atomization and combustion stability. Due to limitations in existing swirl injector models, especially for high vapor pressure propellants like nitrous oxide, an empirical approach was adopted. However, since mass flow regulation is now handled by the upstream venturi, the injector is solely responsible for atomization. This simplification reduces the design complexity and minimizes the need for extensive testing of different geometries.

Ignitor

The ignitor of the combustion chamber plays an important role in the beginning of the combustion process. It has a toroidal shape with a flame guide aimed along the port of the fuel grain, which ignites the fuel evenly along the port length and circumference. The design consists of two C-shaped 3d-printed parts that form a chamber with approximately 75 g of pyrotechnic mixture. It is made from 60 % rocket candy (65 % potassium nitrate and 35 % sorbitol), 25 % magnesium powder, 15 % CaSi powder and 0.5 % iron oxide.

The metal powders produce hot sparks, while the rocket candy functions as both a binder and an expulsion charge. Complementing the chamber structure, a final 3d-printed component acts as a flame guide to help divert the sparks along the fuel port. The pyrotechnic mass is then ignited with four e-matches for redundancy.

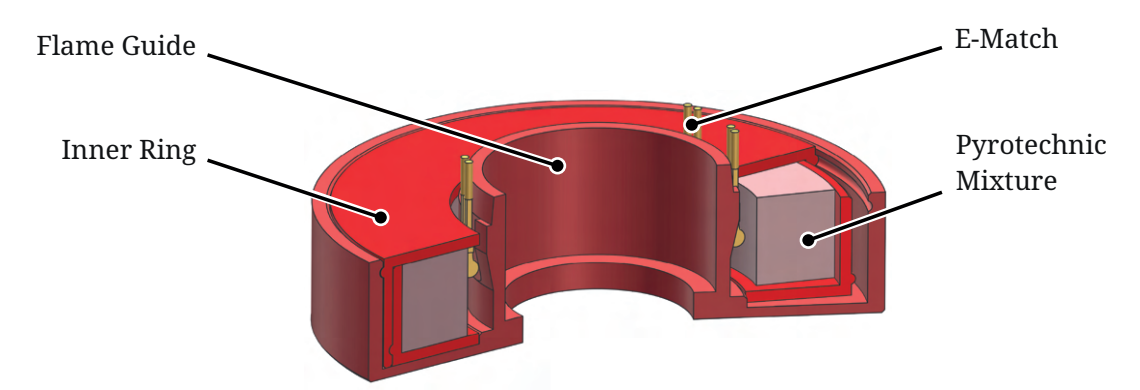


Figure 2.10: Depicted is the ignitor in a cutaway section. The inner ring houses the pyrotechnic mixture, the base allows for four e-matches to be placed and provides the flame guide.





Fuel Grain

The fuel grain is based on a HTPB mixture, cast into a 3d-printed Acrylonitrile Butadiene Styrene (ABS) mold. The fuel composition of the propellant mixture is as follows:

- 90.0 % HTPB
- 9.0 % Isophorone Diisocyanate (IPDI) as the curing agent.
- 1.0 % Carbon black for improved thermal radiation absorption.

To reduce the production time of the fuel grain compared to a more common finocyl core and direct casting into the phenolic cotton insulation tube a test was conducted using a 0.8 mm thin 3d-printed ABS mold. The tests showed promising results and a fuel grain manufactured with this method was already used during the first Hot-Fire day in parallel with the more conventional manufacturing method. The ABS enclosed fuel grain showed no disadvantage compared to the fuel grain cast directly into the phenolic cotton liner. To ensure complete and faster curing, Tris(acetylacetonato)iron(III) (Fe(acac)₃) was added as a catalyst to the HTPB mixture.

Due to a high O/F ratio and a decreasing thrust curve in the initial tests, various additives and geometries were subsequently tested. Aluminum, zirconium, and paraffin powders were each tested as additives at 10.0 % by weight. While all three led to an increase in regression rate of approximately 50.0 %, they also caused a reduction in the engine's overall efficiency. In parallel, a 360° twisted finocyl geometry, with additional twisted side ports, designed to open up during the burn to increase surface area, was tested. The test produced highly promising results, doubling the regression rate and improving the ISP by shifting the O/F ratio closer to its optimal value. This led to the decision to abandon additives and focus on the geometry of the fuel.

The twisted finocyl geometry with side ports underwent four additional design iterations to maximize fuel consumption within the combustion chamber. The final design is shown in Figure 2.11. To improve the performance of the ignitor, the ABS finocyl shell was removed after the HTPB had cured, exposing the fuel.



Figure 2.11: The fuel grain features a advanced twisted finocyl geometry. At the right hand side, the cut was implemented in the plane of one of the side ports to better visualize their swept geometry.



2.2.3 Testing

To verify the performance and reliability of the hybrid propulsion system under development for ISPIDA, a structured Hot-Fire test campaign was conducted. The campaign consisted of eighteen tests in total, eleven horizontal and seven vertical ones. The hybrid engine development began with a series of pressurization system tests, using the previous year's oxidizer tank.

The first Hot-Fire tests served to validate the pressurization architecture under actual load, and to experimentally assess the cavitating Venturi used for oxidizer mass flow regulation. The second batch of tests introduced paraffin wax and aluminum powder as additives to the HTPB. Both resulted in a 50 % increased regression rate. The use of the newly designed grain featuring a twisted finocyl geometry more than doubled the regression rate. This exceeded the intended value and needed further iterations. In the third test cycle, two alternative finocyl configurations were evaluated alongside zirconium powder as an additive. The zirconium exhibited performance characteristics similar to those of aluminum. Additionally, the third test marked the first integration of the new oxidizer tank and fluid subsystem identical to the flight configuration except for the main feed line. The fourth batch of tests introduced new fuel grain geometries once more. However, their performance did not meet expectations.

The fifth cycle of Hot-Fire tests was the first vertical test of the complete propulsion stack in the same configuration as in the rocket. In HF 5.1, the same grain geometry as in tests 4.1 and 4.2 was employed to establish a reliable baseline for comparison. In HF 5.2, a slightly modified version of the grain was tested, yielding improved pressure stability and performance, and was consequently selected for future tests. These tests confirmed the readiness of the first propulsion stack for flight.

The sixth test series served to verify the second propulsion stack's readiness for flight. With two tests completed in the 9 km configuration and one in the 3 km the second stack was deemed viable for flight usage. During the test 6.1 the nozzle ruptured late into the burn. This test is still deemed successful as the flight simulation still predicted an apogee slightly above 9 km. The reason for the rupture is assumed to be a material failure, as no clear evidence was found after the evaluation.

The last Hot-Fire tests were conducted in the course of the all up vertical test. Two Hot-Fires, one in 9 km and in 3 km configuration were done, both successful.

Table 2.2: Summary of the ISPIDA Hot-Fire campaign. F_{max} is the peak thrust, I_{tot} the total impulse, m_{ox} the oxidizer mass and t_{burn} the burn time.

	r	ic omidizer i		urn are sur	
Hot-Fire	F_{max} [kN]	I_{tot} [kNs]	m_{ox} [kg]	t_{burn} [s]	Note
1.1	3.3	23.4	10.3	7.5	New manufacturing method
1.2	3.3	20.5	8.8	6.1	Classic casting manufacturing
1.3	3.4	20.9	9.1	6.1	Classic casting manufacturing
2.1	3.8	27.0	10.3	7.1	Twisted finocyl 1
2.2	3.4	24.8	10.5	8.5	Finocyl with aluminum powder
2.3	3.4	24.9	10.5	8.5	Finocyl with blended paraffin
3.1	3.7	31.5	13.2	9.5	Twisted finocyl 2
3.2	3.6	27.0	11.7	8.0	Finocyl with zirconium powder
3.3	3.7	32.1	13.5	9.5	Twisted finocyl 3
4.1	3.6	31.5	13.5	9.5	Twisted finocyl 4
4.2	3.6	31.7	13.4	9.5	Twisted finocyl 4
5.1	3.7	31.4	13.5	9.5	Vertical, twisted finocyl 4
5.2	3.7	32.1	13.5	9.5	Vertical, twisted finocyl 5
6.1	4.0	29.7	13.5	9.0	Nozzle failure
6.2	4.0	14.7	5.8	3.8	3 km, twisted finocyl 5
6.3	4.0	31.8	13.5	9.0	Vertical, twisted finocyl 5
7.1	4.0	31.4	13.5	9.5	All up vertical, 9 km
7.2	4.0	13.5	5.5	4.0	All up vertical, 3 km



2.3 Aerostructure Subsystem

The rocket's airframe is designed to be as light as possible whilst withstanding aerodynamic and mechanical loads. It can be divided into five main sections, each optimized for a specific function:

- Nosecone: Includes the guidance stack, the parafoil and the PSP.
- Recovery bay: Contains the parachutes and the recovery system.
- Avionics section: Houses the flight computer, payload, pressurant tank, and upper fluid assembly.
- Oxidizer tank: Part of the propulsion subsystem.
- Valvebay structure: Encloses the lower fluid assembly.
- Tailcone: Houses the combustion chamber, the hardpoint of the holddown mechanism, and connects to the fins.

These sections are either connected through coupling interfaces or Radax joints in order to enable straightforward integration of internal subsystems such as the oxidizer tank.

Key features of this subsystem include the integration of the PSP in the nosecone for barometric speed and altitude measurement as well as an actively controlled air brake system in order to enable precise altitude targeting. Furthermore, a holddown mechanism is used to firmly secure the rocket to the launch rail during engine ignition.

All components were dimensioned and validated using analytical calculations and Finite Element Analysis (FEA). Moreover, Computational Fluid Dynamics (CFD) simulations allowed to evaluate pressure distribution, drag characteristics, and flow behavior around key structures. The resulting load cases, covering ten representative scenarios, have been calculated analytically and are documented in the appendix.

2.3.1 Structure

Shell

The material selection for ISPIDA is determined by the desired attributes of the rocket parts. The majority of the shell is wound with Carbon-fiber Reinforced Polymer (CFRP) to ensure low weight and sufficient strength to withstand the forces. In Table 2.3, the lay-up of the REC shell is listed as an example. Furthermore, Glass-fiber Reinforced Polymer (GFRP) is used in some parts of the rocket to provide Radio Frequency (RF) transparency, enabling data transmission of the Control and Telemetry Systems (CATS) as well as the CubeSat. All sections have adequate venting holes to prevent pressure building up.

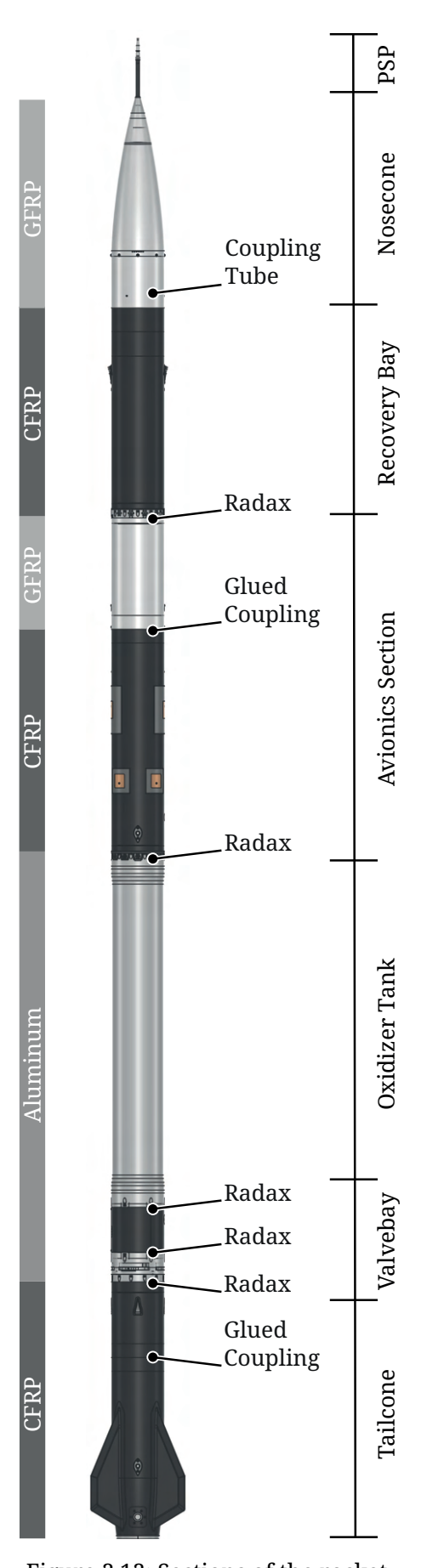


Figure 2.12: Sections of the rocket.



As shown in Figure 2.12, the nosecone and a part of the Avionics (AVI) shell are made of GFRP, the latter at a length of two body diameters. The GFRP part of the AVI shell is connected to its CFRP part by a glued GFRP coupling tube. Additionally, the REC shell and the tailcone are made of CFRP as well. To confirm that the structural integrity under the expected load is given, the classical laminate theory was used with AltairESAComp $^{\rm TM}$. The results are verified via a tube bending test.

Table 2.3: Properties of the wound REC shell.

CFRP	Lay-up [°]	Layer Thickness [mm]
T800	+/- 82	0.4
T800	+/- 45	0.4
T800	+/- 20	0.4
T800	+/- 10	0.4

Radax

Five key connection points within the rocket are implemented using Radax joints. Each joint features a conical interface between the halves, enabling selfcentering and precise alignment during screw tightening. The recovery section is connected to the avionics section. Attached to the avionics section is the oxidizer tank, which transitions at its lower end into the valvebay structure. The air brake is mounted below the valvebay structure and connects at its lower end to the tailcone. Apart from the tank and air brake, each Radax connection is glued to its respective shell with epoxy adhesive. All Radax joints, except for the two located at the valve bay structure, are secured with twelve M4 screws. The valve bay structure itself is fastened with six M5 screws to ensure easier accessibility.

The Radax joint stands out from other alternatives as it only occupies minimal internal space, allowing large interior assemblies to be integrated more easily while maintaining high joint stiffness and low weight. Additionally, the joints provide mounting points, e.g., for the recovery ground plate through an inner flange with screws.



Figure 2.13: Radax connection.

Coupling Tube

The connection of the nosecone is detached from the recovery section at apogee, allowing the deployment of the parachute. This connection is realized with a coupling tube wound from CFRP and a wall thickness of 1.7 mm. The coupling tube is adhered to the REC shell on one end and fits tightly into the inner diameter of the nosecone shell on the other. Additionally, the nosecone is secured to the rocket body with three M2.5 shear pins inserted radially through the nosecone shell and the coupling tube.

Furthermore, two fully adhered coupling tubes are incorporated in the rocket. One coupling tube connects the GFRP part and the CFRP part of the AVI shell. The other connects the cylindrical with the tapered section of the tailcone.



Valvebay Structure

The aim of the valvebay structure's design is to ensure both mechanical stability and easy access to the valvebay, even after the rocket is fully assembled. In order to achieve this, X-shaped struts are used, providing the necessary rigidity while leaving space for accessibility. The structure is mounted on both sides to a female Radax using screws, which not only secures the connection but also helps to center the Radax system.

Finally, the valvebay is enclosed with three carbon fiber panels that are mounted directly to its structure.

Payload Structure

The payload structure is manufactured using Selective Laser Sintering (SLS) 3d-printing and designed to hold one CubeSat. To protect itself and the flight computer from vibrations, the weight of the CubeSat is supported by spring pins. The structure itself is glued to the inside of the avionics shell.

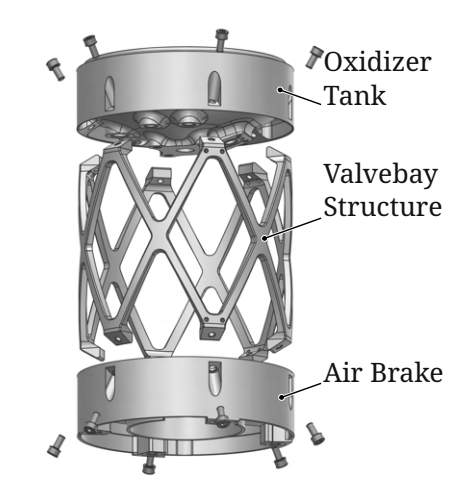


Figure 2.14: The valvebay structure.

Retractable Railbutton

The connection to the launch rail is established using a pair of retractable railbuttons. These railbuttons are equipped with spring-loaded mechanisms that retract the guides upon departure from the launch rail, reducing protrusions from the hull. They are positioned near the rocket's center of gravity and rear section.

2.3.2 Aerodynamics

Nosecone and Tailcone

In order to minimize drag at subsonic and transonic speeds, both the nosecone and tailcone were shaped using a specific profile from the Haack series with a coefficient of C = 0. This geometry, commonly referred to as the von Kármán shape, ensures optimal aerodynamic efficiency in the relevant speed regime. As the same contour is used for the front and rear sections, CFD simulations showed reduced drag as the flow profile becomes consistent. In addition, the manufacturing process is simplified as the same mandrel can be used.

Since the nosecone must be Radio Frequency (RF) transparent, it is made out of GFRP via filament winding. Therefore, it is not possible to integrate the very tip into the winding process. In order to resolve this, part of the PSP assembly contains an aluminum insert completing the aerodynamic shape.

In comparison, the tailcone's curve is significantly shortened to accommodate the nozzle geometry and is designed to fit over the combustion chamber.

Air brake

ISPIDA has an air brake system to control the target apogee, which features four flaps that rotate outwards to increase the aerodynamic drag on the vehicle, allowing the oxidizer feed pipe to pass through it. Therefore, the air brake is placed in the lower end of the hybrid engine, behind the vehicle's center of gravity, ensuring that ISPIDA maintains stability during flight.

The entire mechanism is housed between two aluminum plates featuring custom Radax connections to ensure correct alignment of the air brake and tailcone during assembly. The plates are held together by four titanium M8 screws and house the mechanism, which consists of four flaps and a central gear, driven by a single servo motor placed on top, ensuring that none of the flaps can actuate individually. The gears on the flaps, as well as the central gear, were manufactured using



SLS 3d-printing technology, allowing for more adaptability in the design process and specialized geometries.

The flaps themselves are also made of aluminum and sit on steel shafts, to which the smaller gears are adhered using epoxy. The shafts are mounted inside the plates with two ball bearings, ensuring smooth actuation.

The shape of the control flaps was analyzed in a parameter study. Three aspects were considered in the design: (1) maximum surface area when fully deployed, (2) sufficient contact between the top and base plates to effectively transfer thrust, and (3) minimum surface area inside the rocket that does not contribute to the functionality when fully deployed.

The projected braking power of the air brake is about 500 m in apogee reduction. This value is an estimation based on CFD simulations of the air brake at different deployment states. The simulated drag values were then used in a flight simulation utilizes rocketPy's air brake class. To limit the forces acting on the system, the air brake will only be deployed during subsonic speeds in the coast phase.

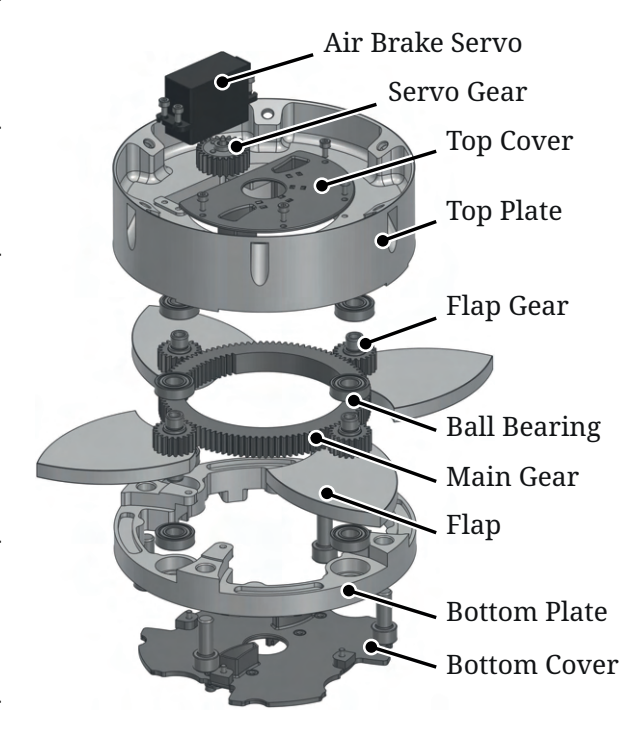


Figure 2.15: Assembly of the air brake.

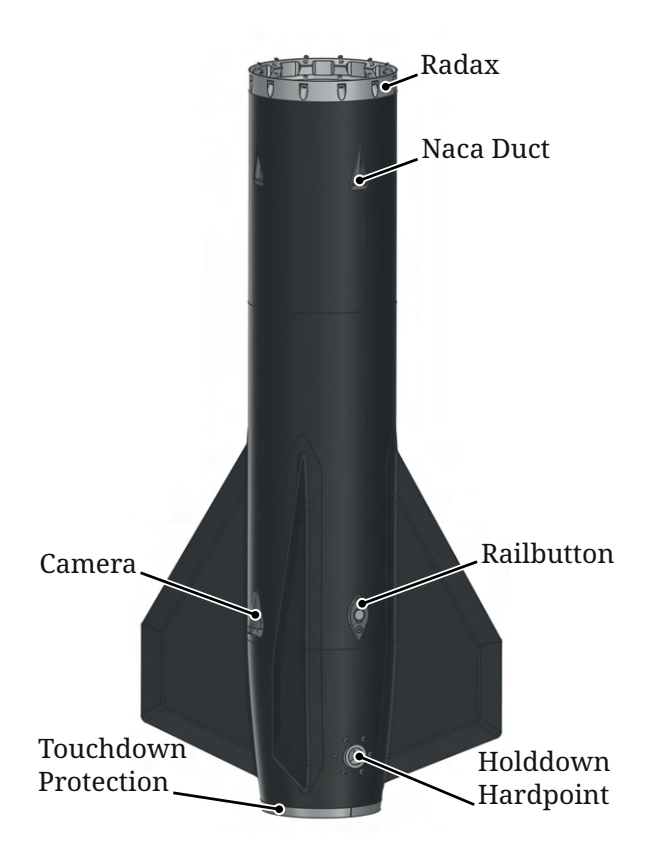


Figure 2.16: Rear view of the fins and the tail section.

Fins

The ISPIDA fins are trapezoidal, with the lower base side of the fin adapted to the curve of the tail section. The fins are optimized in their shape to provide enough area as far aft on the rocket as possible while maintaining a good distance from ground at the lower tip chord edge. It is dimensioned in such a way that they guarantee the stability of the rocket at ground-level wind speeds of up to 10 m/s.

To manufacture the fins, six prepreg layups are laminated onto a prefabricated negative ureol fin mold and after curing, the two halves are adhesively joined together. A liquid-poured resin core made out of a microsphere-resin-solution with 60/40 Vol.% (microspheres/resin) mixing ratio fills the inner gap and ensures structural stability at a low density of $0.58 \,\mathrm{g/cm^3}$ while also allowing for a simple manufacturing process. A flange is integrated into the fin shape, which is bonded to the tail section shell with epoxy glue. Aeroelastic effects were taken into account when dimensioning the fins by calculating their response to the airflow around them analytically with Fin Sim.



Tail Section Heat Management

The upper end of the tailcone features four U.S. National Advisory Committee for Aeronautics (NACA) duct inlets. These use a diverging inlet with a shallow ramp to enhance pressure recovery and mass flow. The sharp inlet edges generate counter-rotating vortices that lift the boundary layer, enabling freestream air ingestion. NACA data shows that these ducts add minimal drag in the transonic regime.

The ducts provide airflow to the tailcone and protect its adhesive joints against the radiant heat from the combustion chamber. The area around the nozzle, which features the hardpoint for the hold-down system, is also protected by a replaceable heat shield. The shield is made out of a Thermoplastic Polyurethane (TPU) 3d-print and layers of cork and aluminum tape. The insulation ensures that the hardpoint for the holddown system is kept below the maximum operating temperature of its adhesive joint during burn time, which has been tested and proven during static hotfire tests.

The TPU 3d-print also protrudes from the rear of the rocket, protecting the edge of the composite frame during touchdown.

2.3.3 Pitot-Static System

The ISPIDA pitot-static system is an experimental system meant to test the achievable accuracy of barometric speed and altitude measurement.

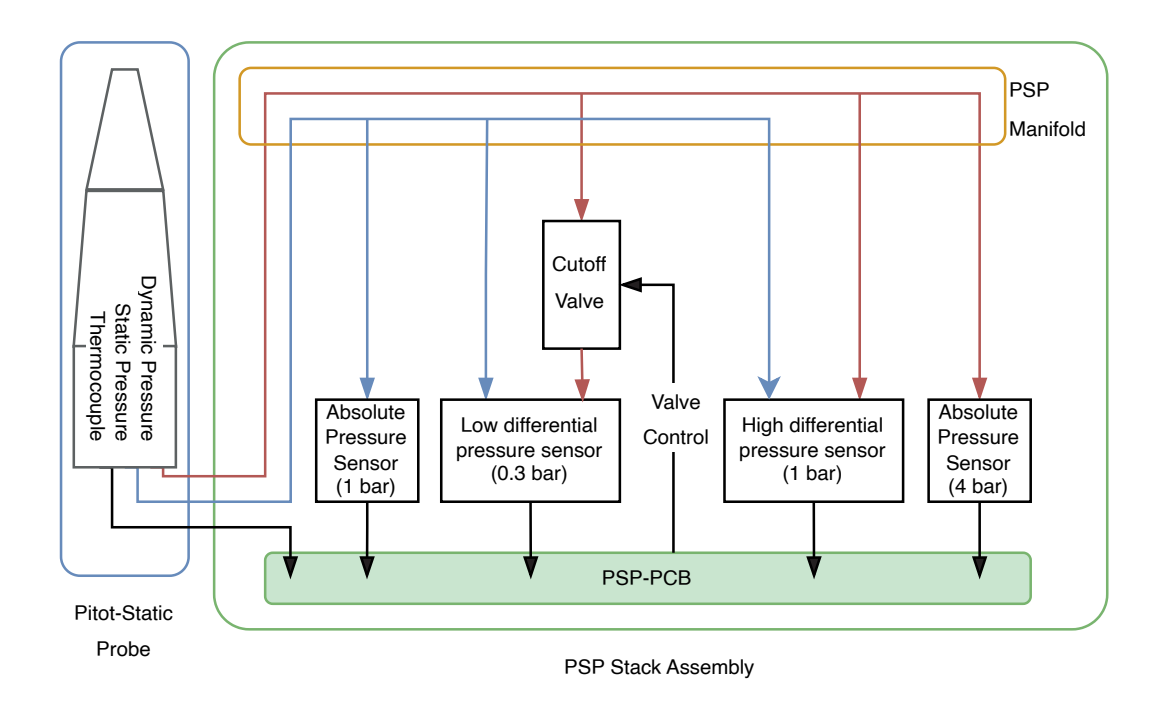


Figure 2.17: Pitot-Static System overview.



Pitot-Static-Probe

The PSP assembly is comprised of a thick-walled carbon fiber tube, a pressure measuring tip, and piping. The geometry of the measuring tip is designed to minimize measurement inaccuracies from the effects of supersonic flow. It is also mounted as far as possible from the nosecone tip, placing the static pressure measuring orifices outside of the bow pressure zone. Due to its fragility, special attention was paid into making the casing of the tip interchangeable. This is achieved by using a low-temperature adhesive for the interface between casing and rear piece, which is permanently bonded to the carbon fiber tube.

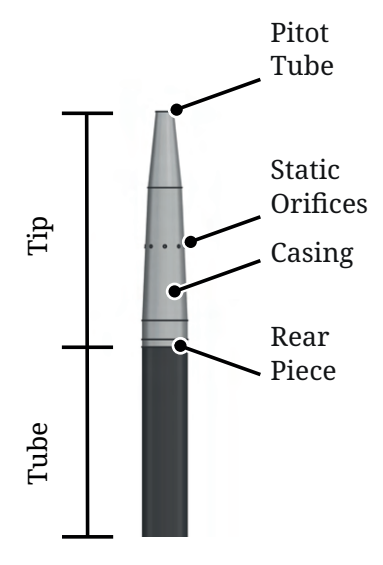


Figure 2.18: PSP tube and tip.

PSP Stack Assembly

Housing both the electronics and mounting hardware, the stack assembly is fastened at the top of the nosecone insert.

The rear of the tube sits inside the cradle with a nylon retention screw locking it in place. Forces on the tube are directly transmitted to the hull via a plastic insert at the front of the nosecone. Said insert also serves to center and align the cradle.

Located behind the cradle is the PSP-Manifold, which distributes static and dynamic pressure to the sensors as can be seen in Figure 2.17.

The cutoff valve is used to protect the low-range differential pressure sensor. The sensor is needed to improve the measurement accuracy at low speeds.

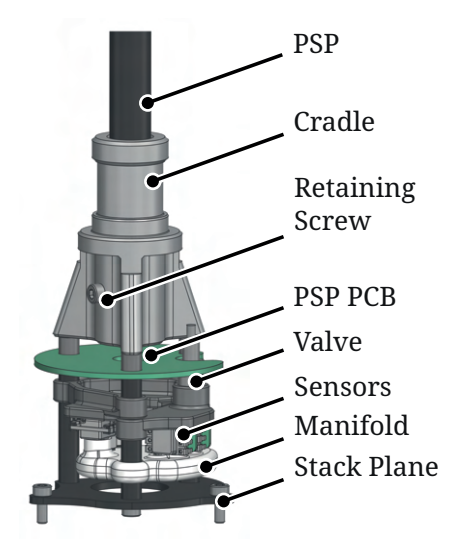


Figure 2.19: PSP stack.

2.4 Recovery Subsystem

A dual-deployment recovery system with two separate parachutes ensures a controlled descent of the main rocket body. At apogee, the first deployment (FD) system separates the nosecone from the main rocket body by pressurizing a designated pressure chamber. This deploys the drogue parachute, which decelerates the rocket to a descent velocity of around 29 m/s. The guided nosecone follows its independent recovery system, as described in Section 2.5. However, if necessary, the nosecone can be connected to the recovery system of the main rocket body. At an altitude of 450 m Above Ground Level (AGL), the second deployment (SD) system triggers the release of the main parachute, further slowing the descent velocity to around 6 m/s for a safe landing.



2.4.1 Overview Recovery Section

The recovery section houses all components and subsystems of the recovery system, as seen in Figure 2.20. The groundplate, located at the bottom, connects the deployment systems and parachutes to the airframe via a Radax interface. The geometry of the groundplate is weight optimized through iterative design studies. It includes cut-outs for cable routing, while still providing mounting points for other components. Mounted on the groundplate are the FD and SD systems, the SD detection, a rotatable eyebolt that connects the main parachute to the main rocket body, and the recovery interface PCB.

Within the recovery section, the main parachute is packed in a dedicated deployment bag positioned above the groundplate, with its connecting lines arranged around the bag. Pneumatic tubes channel the gases released by the FD system into the pressure chamber.

The resulting pressure drives the drogue parachute chamber to shear off the shearpins which secured the nosecone. Parallel to the pneumatic tubes, flexible electrical wiring runs along the recovery tube, providing power and signal transmission to the onboard cameras, the FD detection, and a pressure sensor in the pressure chamber.

To improve efficiency and reliability, the drogue parachute is placed in a dedicated drogue chamber. This reduces the total volume that must be pressurized, thus lowering the required gas quantity for the nosecone ejection while simultaneously increasing the system's Safety Factor (SF).

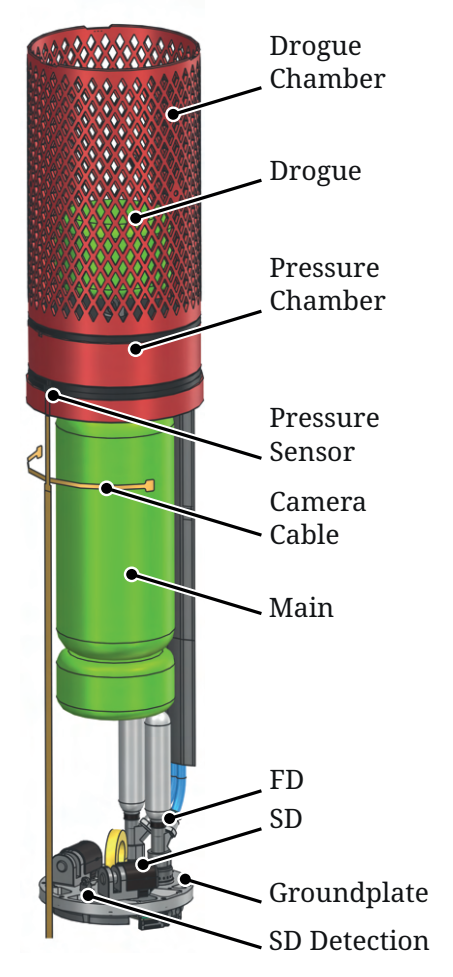


Figure 2.20: Overview of the assembled recovery section.

Pre-Assembly and Integration

The entire REC section is designed to be fully pre-assembled several days prior to launch. Ignitors for the FD and SD systems are inserted from below the groundplate, allowing the REC section in Figure 2.20 to be completely assembled and closed in advance, with ignitor installation deferred until final integration. This pre-assembly significantly reduces the time required for final rocket integration on launch day and lowers the risk of assembly errors under time pressure.

2.4.2 Redundancy

The FD, SD, and Parafoil deployment (PD) (see Section 2.5) mechanisms are implemented with both electrical and mechanical cross-redundancy. Deployment is initiated via electric ignitors triggered independently by both the SRAD flight computer and the COTS CATS. Each deployment unit uses two identical e-matches housed in one titanium chargecup. For electrical redundancy, one ignitor is connected to the SRAD flight computer, the other to the CATS, see Section 2.6.5. For mechanical redundancy, two identical, independent FD, SD, and PD units are installed. Each FD is capable of ejecting the nosecone, even if only one of its two ignitors fires. The main parachute bag is released if either one or both of the SD bolts are retracted. The same applies to the parafoil bag, which opens if either or both of the PDs are triggered.



2.4.3 Chargecups

Each of the deployment mechanisms (FD, SD and PD) has two ignitors in one charge cup, with one ignitor triggered by each flight computer.

Polyurethane (PU) is used to encase the ignitors, which provides an electric isolation against the metal casing, a seal for the ignition gases, and offers mechanical stability as shown in Figure 2.21. This molding enables early assembly of the charge cups, minimizing handling time and reducing the risk of ignitor damage during integration, transport, or flight of the rocket.

Upon activation, only the ignitor head reacts and the PU remains intact, maintaining wire position and isolation, and shielding electronics from ignition byproducts.



Figure 2.21: Chargecup with ignitors molded in PU.

2.4.4 First Deployment

Upon apogee-detection, the two independent flight computers send ignition signals via the interface PCB to the ignitors inside the FD's chargecup. The triggered ignitor (colored red in Figure 2.22) produces pressure, which drives the pin forward. Once a certain distance is traveled, a small hole in the casing is uncovered by the piston, releasing the generated ignitor pressure. Additional explosives, such as black powder, are not needed. The pin pierces the Argon (Ar) cartridge, releasing gas through the sealing plate, pneumatic connector, and pneumatic tubes into the pressure chamber.

The gas pressurizes the pressure chamber, which pushes against the plate of the drogue parachute chamber. This shears off the shear pins, which secured the nosecone to the rocket body, initiating nosecone separation and deployment of the drogue parachute.



Figure 2.22: Sectional view of the assembled first deployment.

A 3d-printed pretentioner prevents the cartridge from loosening under vibration, while a 3d-printed TPU spacer spring ensures that the pin neither pierces prematurely nor remains stuck inside the cartridge. A PTFE plate underneath the pin protects its mating surface from ignition residues. Another feature is the FD cover, preventing any ignition residues from reaching other components in the REC section (visible in Figure 2.23).

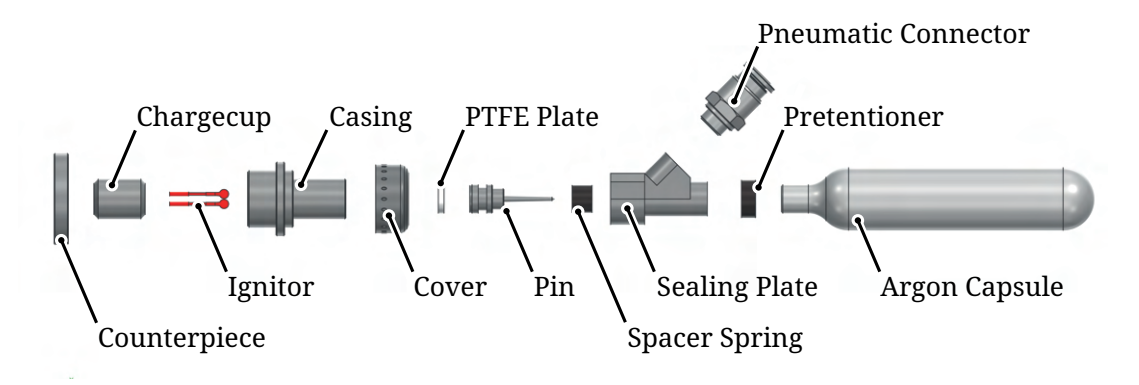


Figure 2.23: Explosion view of the first deployment.





FD Detection

The FD detection uses a linear Hall effect sensor to measure the distance between the pressure chamber and the pressure plate ring. This data is then processed to detect whether deployment has occurred.

Pressure Sensor

To measure the pressure produced by the FD, a pressure sensor is positioned in a small compartment beneath a hole in the pressure chamber. This data is used to verify and validate calculations for the FD during testing and flight.

2.4.5 Second Deployment

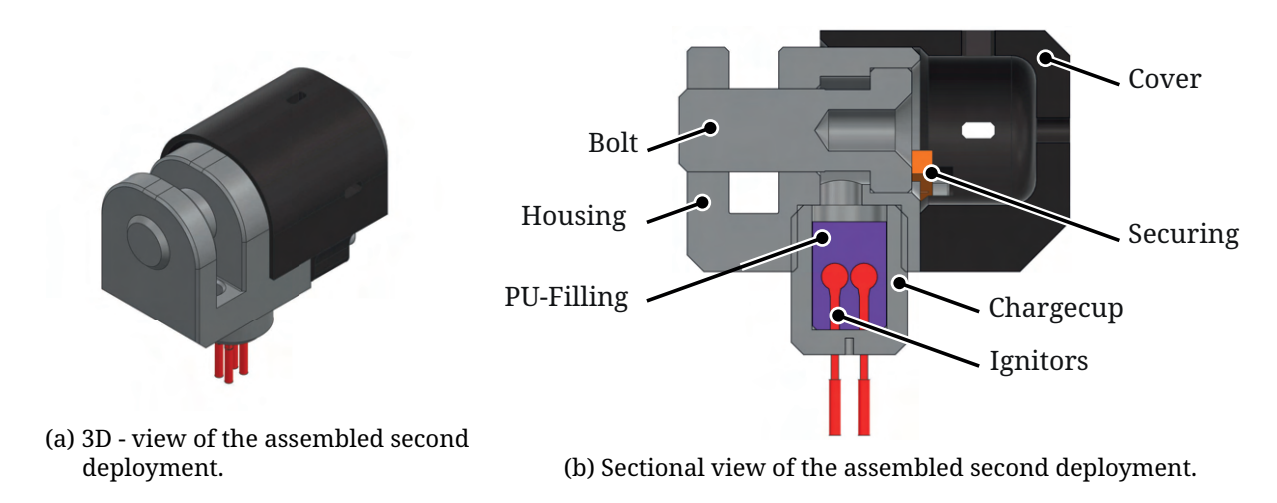


Figure 2.24: 3D and sectional view of the second deployment.

The SD mechanism (Figure 2.24a) constitutes the second stage of the dual deployment recovery sequence and enables the controlled release of the main parachute. It restrains the main parachute in its deployment bag until the target altitude of 450 m AGL during descent is reached. At this altitude, the system releases the bag, allowing the drogue parachute to extract the main parachute.

The SD is mounted on the groundplate of the recovery section. Its primary structural element is a titanium housing, see Figure 2.24b, which serves as the structural anchor and integrates all functional components. Within the housing, a titanium bolt secures the deployment bag via a connection line. The bolt is locked in place by a 3d-printed securing screwed into the housing. This ensures that the pin can only be displaced once the ignitor is triggered, thereby providing a reliable safeguard against premature release.

Upon activation, the ignitor generates pressure. This pressure pushes the bolt out of the housing, shearing off the securing. This releases the SD connection line, which in turn deploys the main parachute bag and allows extraction of the main parachute. The cover captures and secures the bolt within it, preventing uncontrolled movement and maintaining the integrity of the system.





SD Detection

A cable is attached to the main parachute bag and plugged into the groundplate. The flight computer measures circuit continuity and detects any disruption. When the bag is released by the SD, the connector is pulled out, interrupting the circuit and providing a clear deployment confirmation signal.

2.4.6 Parachutes

A dual parachute recovery system is employed, where the smaller drogue parachute is ejected at apogee and the bigger main parachute not higher than 450 m AGL. In Figure 2.25, both parachutes can be seen during a test flight with the lower-mass lower-altitude SPATZ test rocket.

Drogue

The yellow drogue parachute has a cross-shaped design with a total side length of 1.5 m, composed of five square panels with a length of 50 cm, as seen in Figure 2.26a. Its shape was selected for its flight stability, where the cross design outperformed elliptical types in previous projects.

Based on windtunnel tests and previous rocket flights, the drogue parachute has a drag-area product of c_dA = 0.59, resulting in a terminal velocity of $v_{\rm drogue}$ = (29.0 ± 1.5) m/s at 450 m AGL for ISPIDA. At apogee, when deployed into an airstream of 200 m/s, the expected opening shock is $F_{\rm shock,drogue}$ = (5013 ± 180) N.

Main

The elliptical main parachute has a canopy diameter of $3\,\mathrm{m}$, with a top spill hole equal to 20% of its diameter (60 cm). It consists of ten gores and twenty lines, see Figure 2.26b. The shroud lines are 1.5 times the diameter (4.5 m), and each of them is connected to the parachute on a V-lash.

Purple and orange colors were chosen to contrast the blue sky and the white clouds. They also stand out from the ground vegetation, simplifying retrieval operations after landing.

The main parachute was flight-tested with SPATZ test rocket, see Appendix C.15. Data from the test result in a terminal velocity of $v_{\rm main}=$ (5.7 ± 1.3) m/s. When the main parachute is ejected into an air-stream of 46 m/s the estimated shock force is $F_{\rm shock,main}=$ (939 ± 75) N.



Figure 2.25: Drogue parachute and main parachute during descent of the SPATZ test rocket.





(a) Cross-shape of the drogue parachute.

(b) Inflated main parachute during parachute pull-out tests.

Figure 2.26: Photos of the cross drogue parachute and elliptical main parachute.

Main Bag

The design of the parachute bag is adapted from rescue parachute systems used in paragliding. It is manufactured using an aramid fabric, providing high durability and effective protection against sparks and hot gases from nearby deployment charges. The bag is secured by four leaves, each with a central lug (see Figure 2.27a). An elastic loop on one leaf is threaded through the lugs of the others and retained by the main shock cord (see Figure 2.27b). Bag opening occurs when the main shock cord is tensioned during the SD event, ensuring a controlled release.



(a) Main bag opened. The folded main parachute is visible. (b) Main bag closed. The main shock cord seals the bag in place.

Figure 2.27: The main parachute bag once with a folded main parachute inside and once in its closed form.



2.4.7 Parachute Lines and Connections

Swivel Links

To decouple the parachutes and the main rocket body from torsion, rotatable steel swivel links (see Figure 2.28) are used. Swivels are installed for each parachute and connect all the parachute's shroud lines to their respective shock cord. During main parachute descent, the forged steel, rotatable closed-eye eyebolt on the groundplate reduces the torsion introduced by the rocket body into the lines.



Figure 2.28: Rotatable swivel.

Lines

For the connection between the parachutes and main rocket body, polyamide lines were selected for their ability to absorb shock loads through stretching.

To protect the lines from abrasion against the rocket body, aramid-fabric sleeves are added, and metal thimbles are installed to reinforce the spliced loop ends (see Figure 2.29).

A shockabsorber was designed to further reduce loads on the rocket during drogue parachute deployment. Line management was optimized by introducing colorcoded lines, which simplify their assembly and enable quick verification of correct line connections (see Appendix L.1).

Additionally, all line lengths were determined and analyzed using CFD tools, see Chapter K, and verified in flight-tests with the lower-mass SPATZ test rocket.



Figure 2.29: Thimble and rope protection.

Softshackles

Softshackles (see Figure 2.30) are used to connect lines and bolts. They are easy to handle, and, according to testing (see Appendix C.5)), high-strength, making them a lightweight alternative to quicklinks.



Figure 2.30: Softshackle.

Line Management

A detailed schematic of the line management, including all connection points, the placement of the parachutes and their lines, and the lengths of the lines, can be found in Appendix L.1.

2.4.8 Recovery System Tests

The overall testing strategy for the recovery system, including a detailed description of the approach, an overview of all performed tests, as well as all corresponding test reports, can be found in Chapter C.



2.5 Guided Nosecone

BUBO aims to safely land the rockets nosecone independent of the rocket body, at a pre-defined landing point with the help of a steering mechanism and a steerable parafoil. The whole subsystem is equipped with a dual recovery system similar to the main rocket (refer to Section 2.4). At apogee, the nosecone is separated from the main rocket body and deploys its drogue parachute, which then decelerates BUBO to 25 m/s. At 450 m AGL the parafoil is deployed and from this point on the controlled flight phase begins and the whole system steers towards the selected landing point.

2.5.1 Nosecone-Assembly

The guided nosecone consists of three primary components: its shell (refer to Section 2.3.1), the nosecone insert (refer to Figure 2.31), and the PSP (refer to Section 2.3.3). In addition to the COTS and SRAD flight computer, the insert also houses the steering mechanism and the Parafoil deployment. A fan generates active airflow within the nosecone while the rocket remains on the launch pad. Air is exchanged through holes in the shell, ensuring continuous circulation. Special emphasis was placed on modularity and ease of assembly. The complete nosecone insert was designed to be preassembled as a single unit, which could then be secured to the nosecone shell using radial button head screws.



Figure 2.31: Breakdown of the nosecone insert without the PSP.

Steering Mechanism

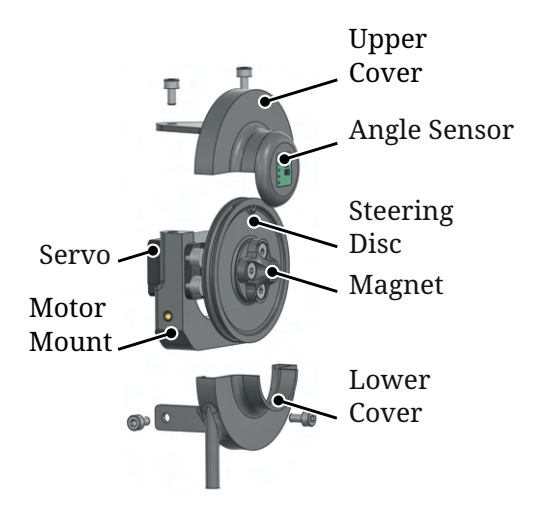


Figure 2.32: Exploded view of the steering mechanism.

The steering mechanism is responsible for controlling the parafoil. Its dual servo design enables independent control of the two outer trailing edges of the parachute. By adjusting the length of the control lines, the curvature of the parafoil in these areas is modified, generating the desired steering response.

One steering mechanism consists of a servo motor, controlled by the Main Guidance Computer (MGC), over a steering disc. These two components form the core of the system. The selected servo motor was chosen for its balance between size and power. Additionally, this type of servo is used in other parts of the rocket, reducing the need for different spare components.

The steering disc is connected to the servo via a servo horn, eliminating the need for adhesive bonding. It is specifically designed to guide the steering line, which is secured by a spliced eye onto a pin pressed into the steering disc. The steering mechanism includes a protective feature that prevents the steering lines from becoming entangled when they are momentarily unloaded.



This protection also ensures that no external interference affects the system and also serves as a mounting point for the angle sensor PCB.

Parafoil deployment

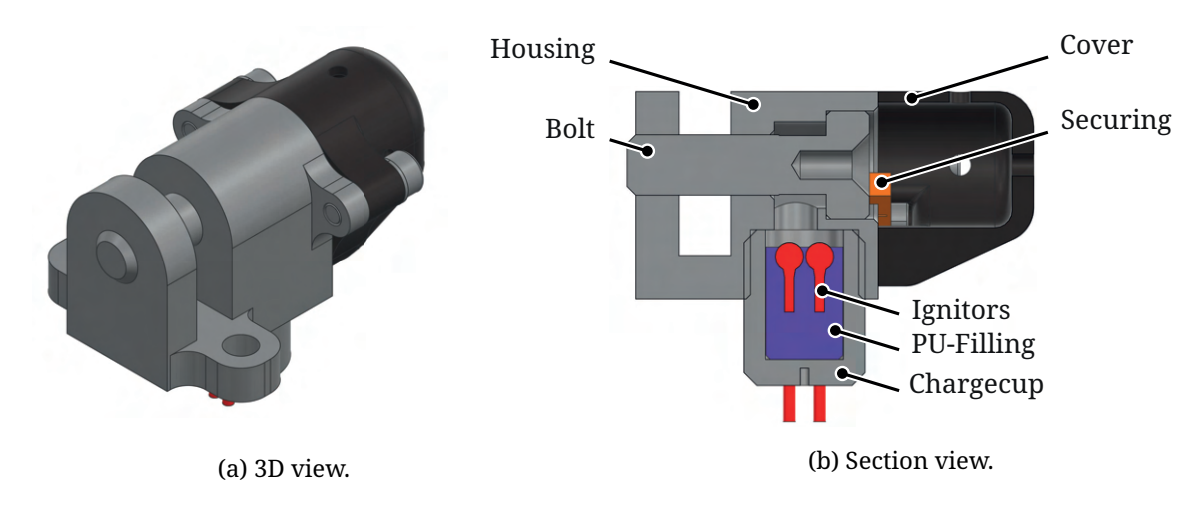


Figure 2.33: 3D and sectional view of the assembled Parafoil deployment.

The Parafoil deployment (PD) (refer to Figure 2.33) functions in the same manner as the second deployment (SD) in Section 2.4.5 and only differs in size, using Finite Element Analysis (FEA)to determine the exact dimensions. For a more comprehensive overview regarding the functionality, please see Section 2.4.5. The same principle of redundancy also applies as for the SD, see Section 2.4.2, Section 2.4.5 and Section 2.6.5.

Flight Computer Hardware

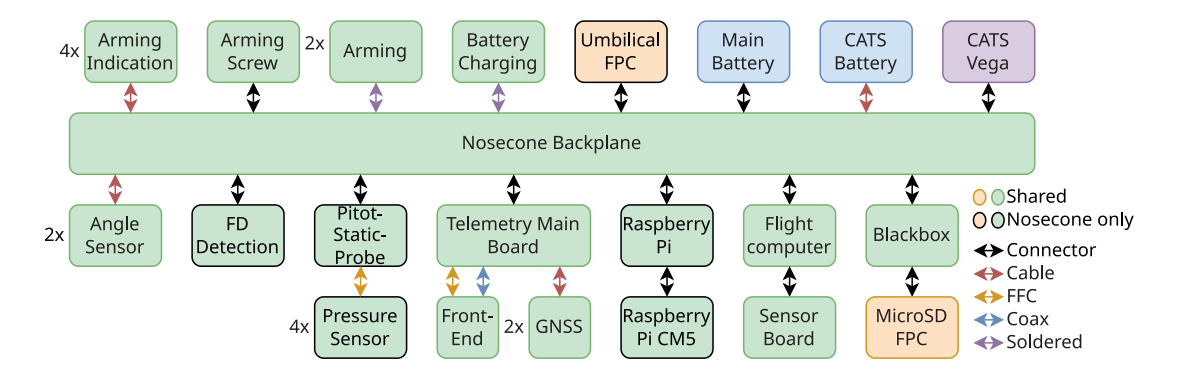


Figure 2.34: All PCBs in the nosecone.

PCBs that are shown in Figure 2.34 and not described in more detail here are identical to those in the rocket, the arming system is also identical, a more detailed description can be found in Section 2.6.

Pitot-Static-Probe PCB

The PSP PCB integrates four pressure sensors, each mounted on a separate board and connected to the main PCB using a Flexible Printed Circuit Board. Through jumpers on the main board, multiple interface formats can be used to read out sensors.





In addition to the pressure sensors, the board incorporates a magnetometer to collect data which aids the calculation of the rockets position. Furthermore, to monitor the temperature of the PSP tip, two thermocouples are used. A digital temperature sensor on the PCB provides data needed to compensate for the thermocouple measurements.

An STM32G473CEU3 processor performs real-time acquisition and processing of all sensor signals, and transmits the processed data via the Controller Area Network (CAN) bus to the backplane.

Nosecone Backplane

The backplane of the nosecone is nearly identical to the rockets. However, some modifications were made to integrate it into the nosecone. The backplane itself is responsible for power distribution and connecting the PCBs of the guidance stack.

The deployment igniters are directly connected to the backplane as well as the angle sensor PCBs of the steering mechanism. In order to easily integrate the PCBs Peripheral Component Interconnect Expresss (PCIes) connectors are in use for the nosecones flight computer, blackbox, and the Raspberry Pi board.

Raspberry Pi PCB

This board serves as an interface between the backplane of the nosecone and a Raspberry Pi Compute Module 5. The Raspberry Pi's purpose is to calculate the flight path of the guided nosecone and communicate it over the CAN bus with its flight computer.

Supporting PCBs:

FD detection The FD detection uses three linear hall effect sensors connected via Flexible Flat Cable to detect magnets embedded in the drogue parachute chamber, similar system in the rocket as described in Section 2.4.4. Three sensors provide system redundancy and fault tolerance.

Parafoil deployment detection The detection of the Parafoil functions in the same manner as the one used for the SD. For a detailed explanation, refer to Section 2.4.5.

Nosecone Umbilical Flexible Printed Circuit Board Connects the nosecone backplane to the USB-C port, which connects to the nosecone's electrical umbilical cable.

Guidance Software

The Main Guidance Computer (MGC) is a Raspberry Pi Compute Module, which is attached to the Main Guidance Flight Computer. An autonomous state detection algorithm is implemented, which is activated by the deployment detection of the nosecone. It then checks the sensor readings for certain ranges and, if the requirements are met, it triggers a state change. A timed overwrite is also implemented if such a requirement is never recognized.

Using parameters given before launch, the system calculates a route towards predefined positions. It uses the readings of the GNSS and AHRS module to estimate a precise location and movement. This data is then used to determine the current flight state and calculate the next control inputs for the servo motors by utilizing a closed-loop system. The requirements have been estimated through tests with our prototype C.23.



2.5.2 Parachutes and lines

Line management

All line lengths of the nosecone were determined according to CFD-analysis. A swivel is installed to decouple the rotational movement of the drogue. Furthermore, a detailed schematic of the line management, including the placement of the parachutes and lines, the length of the lines, and all connection points, can be found in Appendix L.1.

Drogue

In the same manner as the recovery of the main rocket body (refer to Section 2.4.6), the nosecone drogue parachute is also cross-shaped and made out of aramid fiber. The side length of the parachute is 30 cm, where each of the quadratic panels is 10 cm long. The drogue parachute decelerates the nosecone to about (27.0 ± 1.5) m/s at 450 m AGL. The calculations were made according to Section 2.4.6 and a detailed calculation can be found in Chapter K.

Parafoil



Figure 2.35: COTS parafoil during a test flight.

The parafoil (refer to Figure 2.35) is COTS and was originally designed for Radio Controlled (RC) skydivers. The canopy is a ram-air parachute with a rectangular shape. The wingspan is 1.65 m and the cord length is 91 cm. Tests showed that the sink rate can be varied from 5 m/s to 6 m/s (refer to Appendix C.23).

By pulling on one steering line, the corresponding side of the trailing edge is deflected downward. This increases the local curvature of the airfoil, thereby increasing drag on that side. The resulting asymmetry induces a yawing and banking motion, enabling the canopy to turn.

Simultaneously pulling both steering lines leads to a symmetrical deflection of the trailing edges. This action increases the total aerodynamic drag while modifying the angle of attack, which in turn reduces the vertical descent rate and improves horizontal glide performance. This coordinated input reduces the sink rate, achieves a flatter glide path, and optimizes the landing approach.

Small adjustments have been made to enable it to be used in the nosecone. These include extending the risers and the control lines.



2.6 Flight Computer Subsystem

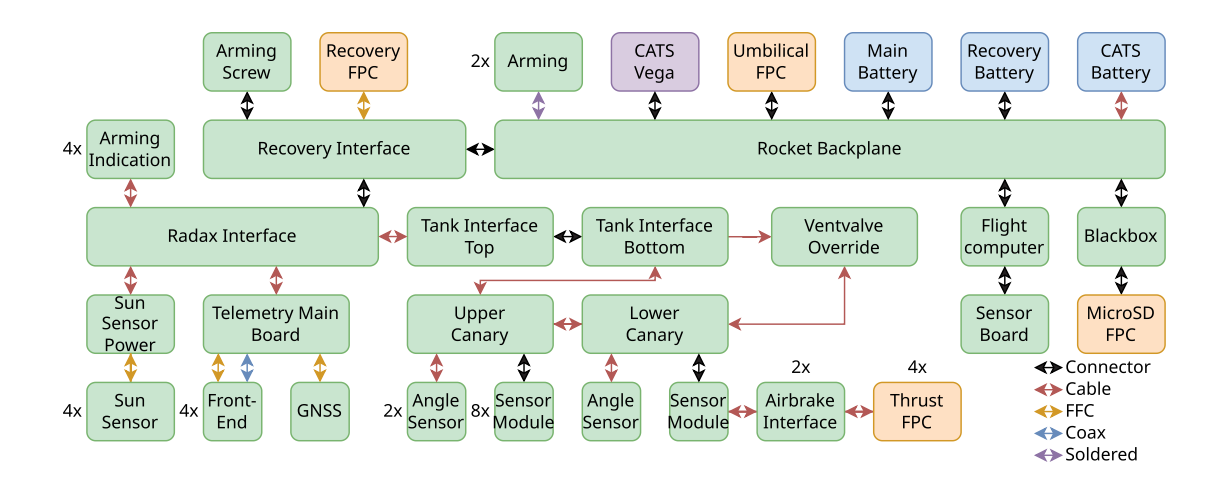


Figure 2.36: All PCBs inside the rocket.

The flight computer subsystem of ISPIDA plays a pivotal role in ensuring successful system operation. Its responsibilities span critical functions, such as controlling actuators in the propulsion system, reading numerous sensors, managing the deployment of the recovery system, actuating the air brake, and handling telemetry for both data transmission and command reception.

Building on the foundation of the flight computers used in previous projects, this latest iteration integrates several previously established and reliable features, including an SD card encased in CFRP used as a blackbox, an integrated cooling solution, and the powerful STM32 Microcontroller Unit (MCU) at its core. In addition to these proven components, the system incorporates several new developments and optimizations, further enhancing its capabilities.

A CAN bus is used to connect all MCUs inside the rocket to each other. This has the advantage that all nodes can communicate directly with each other, enabling decentralized data handling and better rocket control. It also enables the use of a single shared protocol, making development and testing easier.

Most cable connections between sections were replaced with blind mating PCB edge connectors placed inside the Radax connections. This makes rocket integration much faster, as no cables need to be connected separately before the mechanical connections are made. Additionally, all important connections use at least two redundant pins inside the connectors.



2.6.1 Power System

Power Distribution and Management

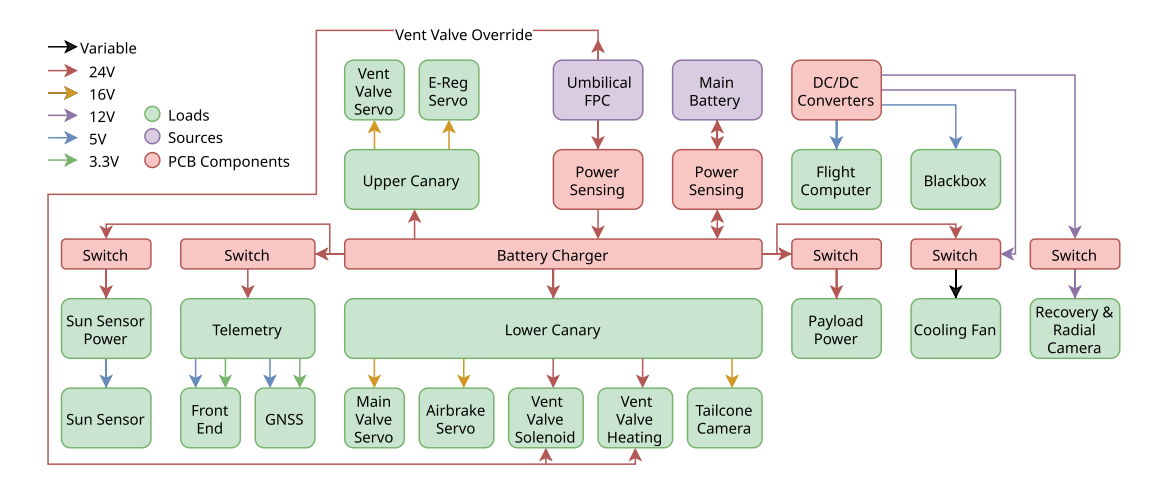


Figure 2.37: Power distribution overview.

The power distribution and management system, shown in Figure 2.37, outlines the primary power flow within the rocket, excluding the recovery system. It includes the main battery, internal electrical umbilical PCB, and various subsystems connected via the main power bus on the backplane. It incorporates voltage and current sensors, enabling real-time monitoring of power consumption and battery charging status for both the system and the battery.

This setup ensures reliability by automatically switching between external and internal power sources. During flight, when external power is unavailable, the system seamlessly transitions to the internal battery. The figure also shows the electrical independent connection of the vent valve override, which enables safe venting of the rocket's tank, even if all internal electronics fail.

Battery Pack

The primary power system for the rocket is a custom-built battery pack that includes two sections: a 6S (six cells in series) 18650 Lithium-ion (Li-ion) battery, which powers the main rocket systems, and a 2S (two cells in series) 18650 Li-ion battery dedicated to the SRAD recovery ignition system. The main battery, with a capacity of 3500 mAh, is designed to support full rocket operations for a minimum of three hours. The battery pack, shown in Figure 2.38, integrates a battery management system to ensure safe and efficient charging of the main battery cells. Additionally, the electrical umbilical cable allows for power supply and battery charging during pad standby to extend operational readiness.



Figure 2.38: The battery pack.

Cable Management

To ensure safe operation under all conditions, internal rocket cables utilize UL1332 specification with Fluorinated Ethylene Propylene (FEP) insulation, rated for the complete temperature range expected during operation. Additionally, all connectors use either integral locking mechanisms or are mechanically secured with screws during assembly to prevent inadvertent disconnection. To enable easier assembly, all cables requiring connection during assembly employ blind mating





connectors within the Radax connections, and all cables are secured with cable ties to provide strain relief.

2.6.2 Avionics Stack

The avionics stack is the main avionics assembly that includes critical components such as PCBs, batteries, and subsystems like the flight computer and recovery systems. Designed to create a compact and reliable system, the avionics stack reduces internal wiring complexity while ensuring strong performance during flight. This integration allows for efficient testing and easy access to all components before final rocket assembly, as shown in Figure 2.39.

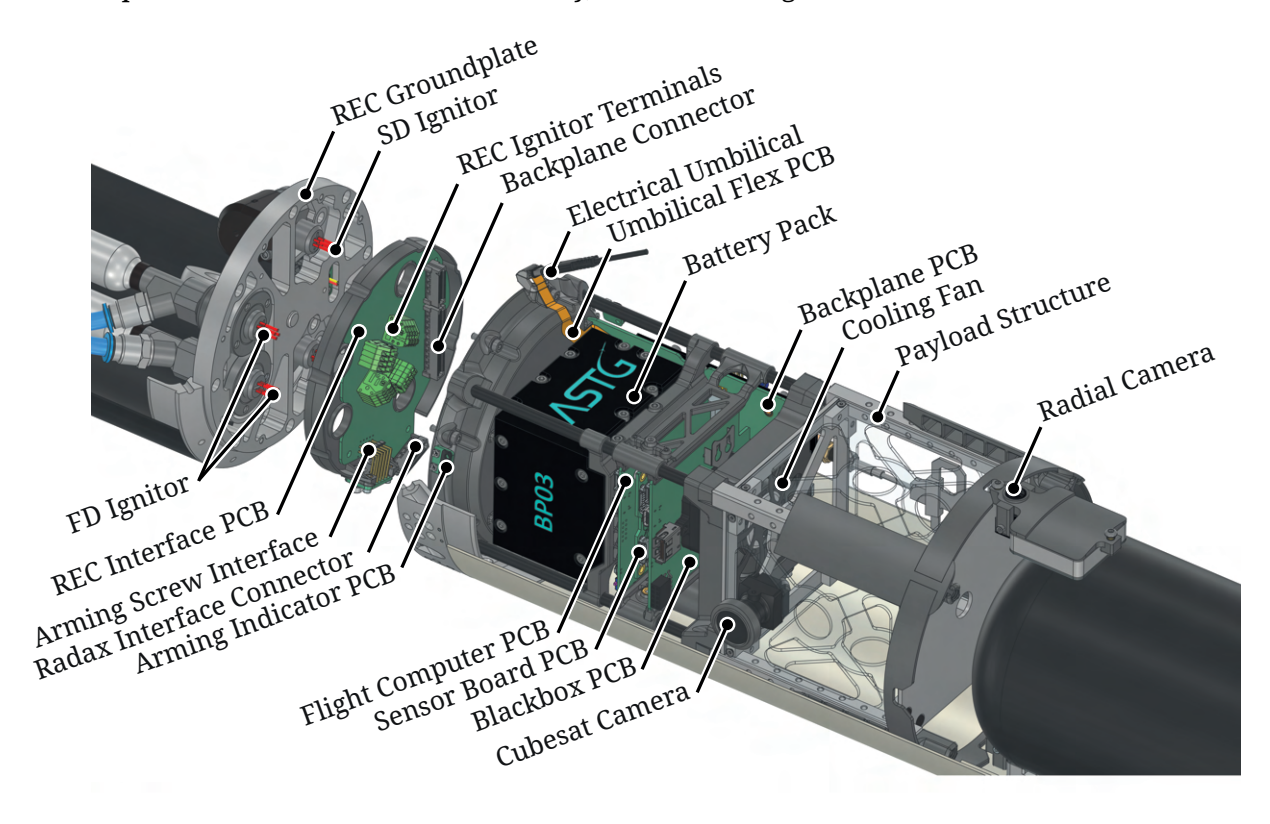


Figure 2.39: Overview of the avionics stack and its components, including the avionics mount, and the payload structure.

A key part of the avionics stack, the avionics mount, supports all components securely and interfaces with the recovery system. It holds PCBs, batteries, and cables in place while connecting to the centering ring at the bottom of the structure to prevent lateral movement. The overall system design, depicted in Figure 2.39, ensures that the avionics stack integrates seamlessly with the other subsystems. Positioned on the lower side of the avionics mount is the payload structure which hosts the 1U payload of the rocket.

The avionics mount is 3d-printed from nylon, reinforced with carbon tubes, and designed with airflow channels for cooling. The backplane is mounted on the avionics mount and serves as the central interconnect for subsystems, supporting standardized form factors for the flight computer PCBs. This design enables easy and flexible swapping of PCBs when testing or replacement is needed due to a malfunction. The main flight computer and the blackbox PCBs are designed to fit the PCIe slots of the backplane and are secured with two bolts, ensuring a stable connection during flight.

As shown in Figure 2.39, the REC interface is mounted on the REC groundplate and is responsible for connecting the ignitors. After the ignitors are connected, the avionics stack can be secured to the REC groundplate via the edge connector on the backplane and fastened with bolts. Once fully



seated, the cubesat mounted on avionics stack rests within the cubesat mount, ensuring stability and minimizing lateral movement.

2.6.3 Avionics Stack PCBs

Main Flight Computer

The main flight computer, shown in Figure 2.40, is a critical component of the rocket's avionics system, responsible for data acquisition and system control. Powered by an STM32H745ZIT3 MCU, it integrates a 3.3 V regulated voltage supply. This year's iteration features an interface to a smaller sensor board PCB, which hosts flight-critical sensors. The main flight computer connects directly to the backplane via a PCIe interface, ensuring reliable communication and power supply, simplifying overall system integration.



Figure 2.40: Main flight computer.

Sensor Board

The Sensor Board PCB serves as an extension to the main flight computer. It hosts critical sensors like a MS5607 barometer for precise pressure measurements down to 10 mbar as well as a BMI088 IMU for accurate inertial sensing. The board also hosts an IAM-20380 gyroscope, an AIS2IH1 accelerometer, and a BMP390 barometer for additional data acquisition. All sensors are duplicate and connected to the MCU via separate Serial Peripheral Interface (SPI) interfaces for better redundancy.



Figure 2.41: Sensor Board.

Blackbox

For ISPIDA, the blackbox was redesigned with a dedicated PCB, featuring a real-time clock for precise timestamps on all data packets stored on the SD card, which is encased in CFRP. The real-time clock is powered by a rechargeable Li-ion button cell battery. The blackbox integrates its own STM32 MCU and CAN bus transceivers to monitor both CAN buses in the rocket. As a redundancy measure, it also connects to the main flight computer via Universal Asynchronous Receiver Transmitter (UART) protocol, ensuring all flight-critical data is reliably logged to the SD card. In order to easily access the data, it is possible to connect a Universal Serial Bus (USB) thumb drive to the PCB and copy the stored data.



Figure 2.42: Blackbox.



Backplane

The backplane PCB, illustrated in Figure 2.43, runs throughout the length of the avionics mount and serves as the central interconnect for all components. It features PCIe connectors, battery sockets, and various other connections, which facilitate efficient and organized wiring within the rocket. Additionally, it hosts a combined buck-boost battery charger, the LTC4020, which ensures stable power management. This design minimizes the need for additional cabling and provides a reliable, compact, and easy-to-assemble avionics stack. In order to optimize space, the COTS CATS Vega is mounted onto the backplane via pin headers. The necessary wiring and traces of the CATS on the backplane are independent of any SRAD components. The SRAD and COTS arming PCBs are similarly mounted onto the backplane.



Figure 2.43: Backplane.

Arming PCB

The arming PCB features four identical redundant circuits, each containing two input comparators, one Flip-Flop, and one p-channel MOSFET. The comparators compare the arm and disarm signal levels to a fixed reference voltage. When exceeded, the Flip-Flop switches accordingly and directly controls the MOSFET. The four MOSFETs are arranged in a 2x2 configuration with two in series per branch and two branches in parallel, ensuring full functionality even if one circuit fails. All sub-circuits are individually fused. The four arming and disarming inputs connect to two redundant cable pairs in a way that allows disarming even if one cable breaks, while preventing arming.





Figure 2.44: Arming PCB

Recovery Interface PCB

This PCB is used to connect the backplane with the rest of the rocket electronics through an edge connector placed inside the Radax. This connector mates automatically with a PCB placed inside the Radax of the avionics section, when the rocket is integrated. In addition, the recovery interface also hosts the connectors for the recovery ignitors, the SD detection, and the arming screw switch PCB. The recovery Flexible Printed Circuit Board is also connected to it using a Flexible Flat Cable. A magnetometer, used for improved attitude determination, is also positioned there, maximizing its distance from high-current circuits that generate magnetic interference.



Figure 2.45: Recovery Interface.

Electrical Umbilical Flexible Printed Circuit Board

The electrical umbilical uses a USB-C with custom pin-out to provide all necessary electrical connections while the rocket is still on the launch rail: 24 V power, engine ignition signal, reset input/output, vent valve override input, four arming channels (two each for SRAD and COTS recovery systems), and four corresponding disarming channels. The USB-C plug is soldered on a Flexible Printed Circuit Board which is connected to the backplane of the rocket.



2.6.4 Supporting PCBs

Several other PCBs are used throughout the rocket:

- **Recovery Flexible Printed Circuit Board**: Houses the pressure sensor in the pressure chamber and the FD sensor; powers cameras in the recovery section.
- Radax Interface: Connects avionics section cables to the recovery interface PCB during rocket integration.
- Tank Interface Top: Links avionics section cables to the tank interface bottom PCB during integration.
- Tank Interface Bottom: Connects the tank interface top PCB to the upper and lower canary via cables.
- **Arming Screw**: Two M3 screws to mechanically disconnect battery power from recovery electronics.
- **Arming Indication**: Two Light Emitting Diodes (LEDs) indicating the arming status of the rocket or nosecone.
- Angle Sensor: Measures absolute actuator angle using an AS5600 sensor.
- Ventvalve Override: Enables solenoid valve actuation with an external voltage.

Sensor and Control Nodes CANary

The CANaries are SRAD PCBs that both sample sensors and control actuators while communicating with the flight computer via CAN bus.

The eight sensor channels can be configured individually for either thermocouples, pressure, or strain sensors. This approach allows maximum flexibility in later design decisions and a wide range of applications of the same hardware. In the same sense, a CAN bus was chosen for virtually unlimited expansion potential.

Each CANary board is equipped with two types of actuator controls: two Pulse-width Modulation (PWM) channels with adjustable voltage supply for servo outputs, and three high-power digital outputs for other types of actuators.



Figure 2.46: The CANary PCB.

Sun Sensors

The sun sensors will help determine the attitude on both ISPIDA and project APEX. The system consists of two main components: the sun sensor PCB (Figure 2.47) and a breakout board.

There are four sun sensor PCBs connected to each other in a ring around the body of the ISPIDA rocket - this ensures that at least one sensor has a direct line of sight to the sun. Each sun sensor has a single two-dimensional PSD (placed on the underside of Figure 2.47) that is used for determining the characteristics of the incoming light ray, such as its vector, angle, and total intensity. To ensure that the PSD receives only a tightly confined beam of light at any given moment, it is covered with a 3d-printed light-blocking cover with a 0.2 mm pinhole, which is attached directly to the sun sensor PCB.

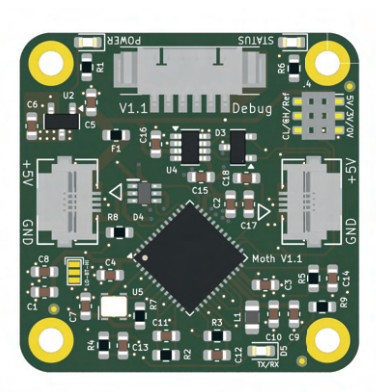


Figure 2.47: Sun Sensor PCB.



2.6.5 Recovery Electronics

The primary purpose of the recovery electronics is to reliably actuate the FD and SD of the recovery parachutes. Figure 2.48 provides an overview of the components responsible for these deployments. The CATS Vega is used as the COTS flight computer for recovery electronics, as it is already required to be included for tracking. Together with the SRAD main flight computer, the two systems provide the necessary redundancy for the recovery deployment. The diagram illustrates the complete cross-redundancy of the system, where each flight computer can trigger each deployment.

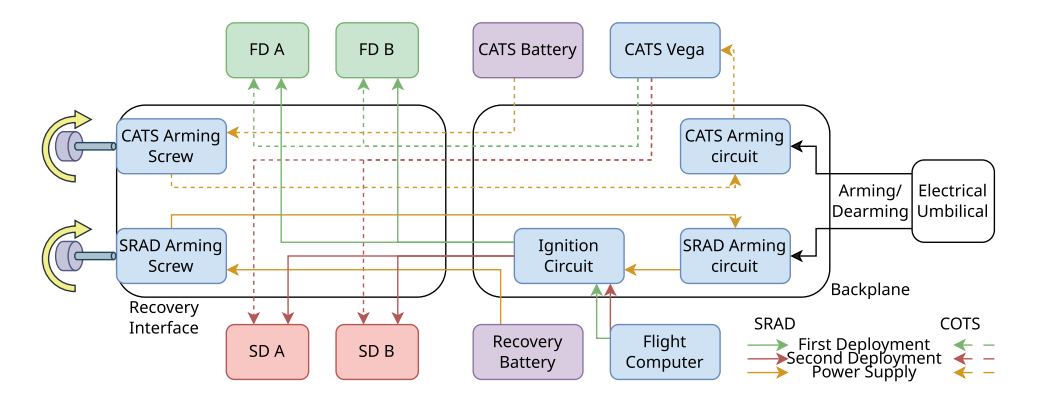


Figure 2.48: Cross redundancy of the recovery system triggered by COTS flight computer and SRAD main flight computer.

Arming System

Due to ISPIDA's propulsion system length preventing ground access to the avionics stack and nosecone, a cable-based, fully redundant arming system was developed using the USB-C umbilical cable to provide arming and disarming signals.

The system features two mechanical screw switches secured with hex keys through designated access holes. When connected, these switches supply power to the arming PCBs, which are described in detail in Section 2.6.3. From the arming PCBs, power is supplied to the SRAD and COTS recovery electronics.

The recovery interface PCB acts as a passive connector, routing pyro-channels to terminal blocks for igniter connections. All connections between the recovery interface, arming screws, and backplane are redundant, using at least two connector pins placed in opposite directions.

The main flight computer continuously measures igniter resistance through dedicated sensing circuits to verify proper igniter connections and detect wire breaks or short circuits before and during flight operations. The SRAD igniter circuits are controlled by two independent MCU Input/Output (I/O) pins each, with separate MOSFETs for each igniter, providing four independent ignition channels in total.

Arming Feedback

To provide feedback about the arming status of the rocket, multiple separate methods are used:

- A small voltage, well below the arming threshold, is applied to the arming input connection and activates an indicator light inside the safety control box.
- Multiple bright red LEDs that light up if any system is armed, are placed around the circumference of the rocket
- Each flight computer has an audible alarm to indicate if it is armed



 All arming voltages are measured and the values are sent over telemetry to the mission control

2.6.6 Flight Computer Software

The software for the ISPIDA flight computer is built on a custom SRAD Real-time Operating System (RTOS) known as RavenOS. This RTOS, derived from SmartOS[2], is specifically tailored for use in ASTG projects. Developing a custom RTOS allows for system optimization to meet specific hardware and functional requirements, resulting in a significantly smaller codebase and reduced runtime overhead. The primary core of the STM32H745ZIT3 MCU is dedicated to running the main software, while the secondary core is assigned to handle sensor reading and processing tasks. Communication between these cores is done using a shared memory partition, where the corresponding core is notified via an interrupt if new sensor data is available.

The main core's software is organized into distinct tasks, each dedicated to a specific system functionality. This modular approach facilitates the development of well-structured code that is easily reusable across multiple projects. The benefits of this design are apparent when comparing the state diagram of the flight computer software for the rocket with that of the Filling Station (FS), as shown in Figure 2.49 where several software states are nearly identical.

The sensor core's software continuously reads the sensor board's data via SPI. After each full reading, meaning reading all sensors once, an iteration of the altitude and attitude calculation is done, which is discussed further in Section 2.6.6. Sensor and filter data are then written to the shared memory partition using hardware semaphores for simultaneous access protection.

With the ability to target either 9000 m or 3000 m, the flight computer software can be configured into corresponding modes that affect the automatic state detection and Air Brake Actuation. The current mode is displayed in the mission control to check the correct selection.

State Machine

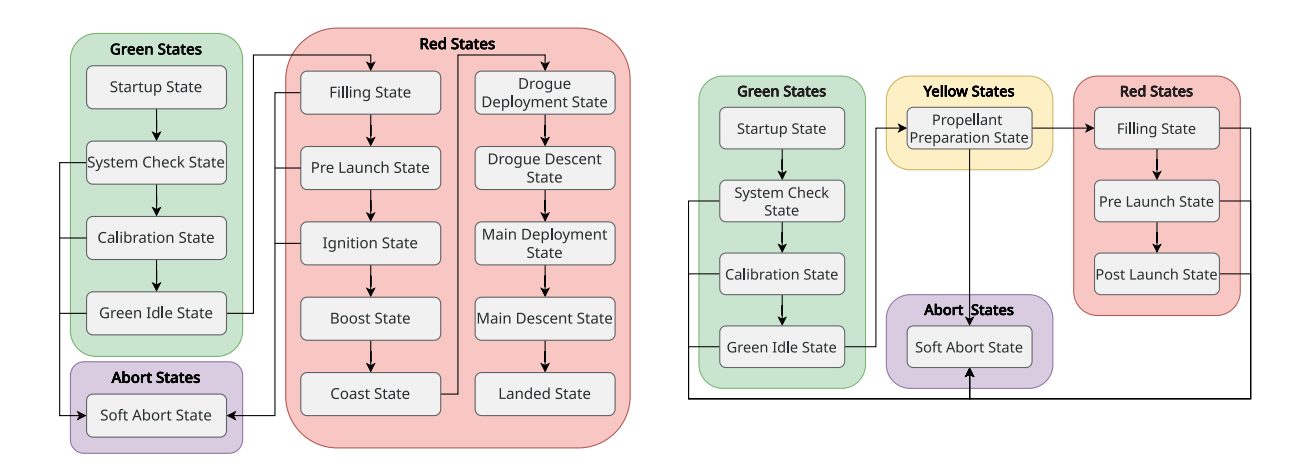


Figure 2.49: State diagrams of the SRAD flight computer: left – rocket, right – filling station.

The various states of the rocket's flight computer software are illustrated in Section 2.6.6. These states are categorized into green states, where the rocket is safe to handle, and red states, indicating that the rocket may be filled with fluids. Upon startup or after a reset, the flight computer initializes in the startup state. During the system check state, all components in and around the rocket undergo thorough checks. Once these checks are completed, the starting height and orientation are calibrated in the calibration state. Following calibration, the rocket enters the green idle state, where it remains until the FS is ready for the Filling State.



During the filling and pre-launch states, the rocket and FS are synchronized, ensuring they remain in the same state and can only progress to the next state simultaneously. In the pre-launch state, the launch sequence is initiated.

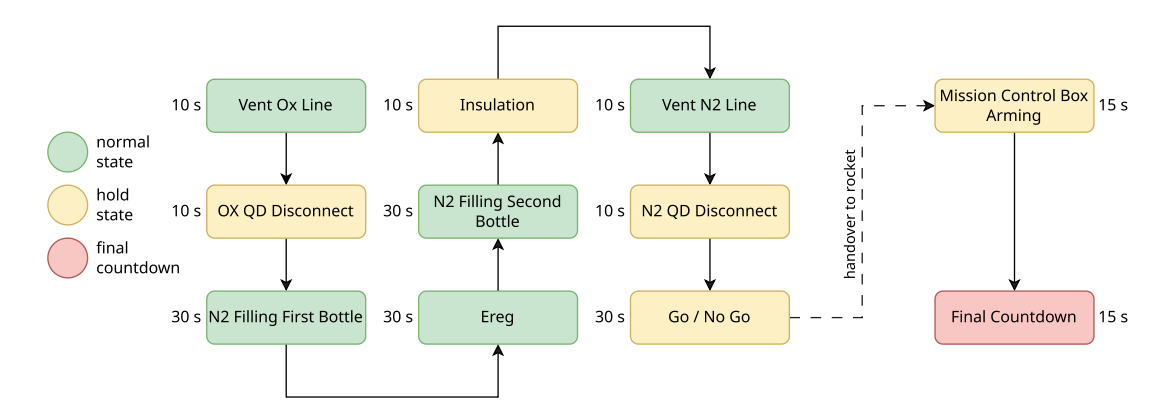


Figure 2.50: The launch sequence with all states, their durations, and transitions.

The launch sequence is designed to minimize user error and automate the final launch procedure. When initiated during the pre-launch state, the FS begins the sequence as seen in Figure 2.50. Throughout the sequence, holds are implemented at steps where completion may exceed the expected duration. These holds, marked in yellow, pause the sequence if step confirmation is not received within the predetermined time window. Additionally, the mission control officer can manually hold the sequence at any time. These holds have to be manually advanced by the press of a button in the mission control. At T-30 s, control is handed over to the flight computer and it transitions to the ignition state. Before the final launch, the mission control officer has to confirm one last time that everything is ready for launch by arming the mission control box and pressing the ignition button. With this, the final countdown starts, leading to the launch.

The countdown can be canceled by flipping the abort switch on the mission control box, which keeps the flight computer in the ignition state, allowing the countdown to be restarted if necessary. If any unexpected events occur while the rocket is on the ground, the flight computer can be transitioned to the soft abort state. In this state, all actuators, except the engine ignitor, can be controlled by the mission control, ensuring that the rocket can be brought into a safe state.

When everything functions as intended and the rocket lifts off, the automatic state detection, as described in Section 2.6.6, takes over. This system advances the rocket through the subsequent states until it reaches the landed state.

Automatic State Detection

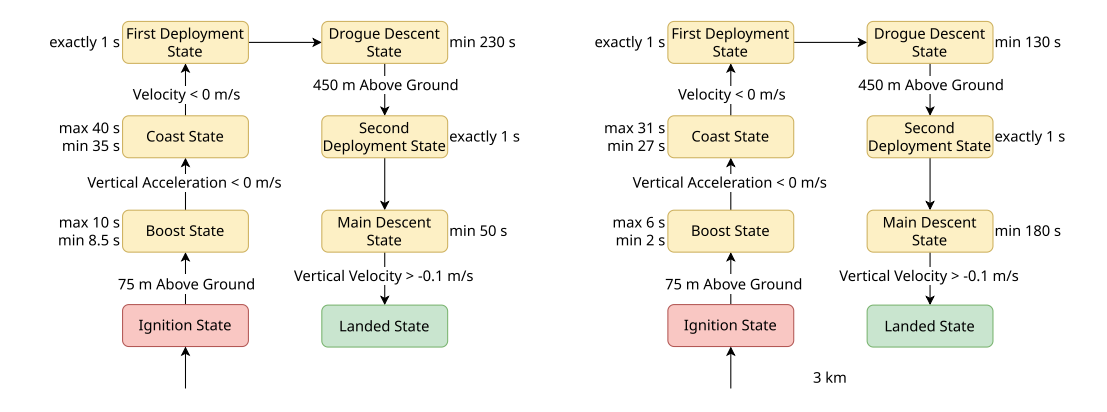


Figure 2.51: Automatic state detection for 9 and 3 km flights.



Technical Report



The automatic state detection system is responsible for seamlessly transitioning the rocket from one state to the next during flight. Figure 2.51 illustrates all possible states and the specific conditions required to advance to the subsequent state. Certain states are also assigned a minimum duration to prevent premature transitions caused by sensor noise during critical events such as parachute deployment or engine ignition. Additionally, a maximum duration is enforced to ensure that issues like frozen sensor data do not hinder the progression to the next state. According to the set target height, different predefined durations are chosen. To make the most precise decision, a Kalman filter is deployed to calculate the attitude described in Section 2.6.6.

Filter for Altitude and Attitude Calculation

To calculate the altitude, data from two barometers and two IMU units are processed using an extended Kalman filter. The filter predicts altitude and vertical velocity from accelerometer measurements and corrects the prediction with barometer readings. Gyroscope measurements propagate quaternions for each IMU, which rotate the accelerations from body to earth coordinates. The four transformed accelerations are averaged, and gravity is added to compute the net vertical acceleration. Each barometer measurement is combined into a two-dimensional vector, and the measurement covariance is scaled based on the relative size of the residuals to reduce the influence of faulty readings. The state and covariance matrices are updated using standard EKF equations.

Additionally, an experimental extended Kalman filter is being tested to estimate the rocket's attitude, which is represented using a quaternion. The prediction step utilizes IMU data, and the filter is subsequently updated with measurements from the magnetometer and sun sensors.

Air Brake Actuation

The air brake control software is utilizing the same concept as in past projects. The goal of the control software is to deploy the air brake in a smooth and precise manner. The controller actuates the air brake according to the calculations made by the apogee estimation software, which takes the current speed, height, current air brake status, and target apogee to determine the correct actuation. The air brake software can be configured for a target apogee of either 9000 m or 3000 m.



2.7 Telemetry Subsystem

The telemetry system of ISPIDA enables communication between the rocket, mission control, and the GSE. It uses two independent 2.4 GHz LoRa links: one from the rocket body and another from the nosecone, both transmitting to the mission control. The nosecone works as an independent landing vehicle, so it requires its own communication link.

All telemetry nodes use the same hardware. The main board includes an STM32H745 MCU and a Semtech SX1280 transceiver. Inside the rocket, the board connects to the CAN bus for communication with the flight computer and other subsystems. A separate Global Navigation Satellite System (GNSS) board is added, which carries two GNSS modules to provide redundant and reliable position data. On the receiver side and in the FS, an Ethernet PCB with Power over Ethernet (PoE) is connected to provide a connection to the mission control server.

The firmware is built on FreeRTOS and follows a modular design. This allows the same software to be used in different places: the rocket, mission control, and also the GSE. On the rocket, patch antennas are placed on the outside, so no RF-transparent materials are needed around the SRAD telemetry hardware. Two antenna systems are used: one for LoRa at 2.4 GHz and one for GNSS in the L1 band.

2.7.1 Patch Antenna System

The antenna system on the rocket uses a total of six patch antennas, all mounted on the outside of the rocket body. For the 2.4 GHz SRAD LoRa link, four patch antennas are installed in a ring around the avionics section. In addition, two SRAD GNSS patch antennas are used to receive signals for the GNSS system.

All antennas are placed externally on the carbon fiber tube. Each 2.4 GHz antenna connects directly to a frontend PCB mounted just behind it on the inside of the tube. The GNSS antennas are connected directly to the GNSS PCB. Because no antennas are placed inside the avionics shell, the lower section can be built entirely using carbon fiber.

2.4 GHz Antennas

The LoRa system uses four identical righthand circular polarized patch antennas, each with a gain of 6 dBi. Mounted in a circular arrangement, they combine to form a uniform radiation pattern of 3 dBi. This patch ring ensures even coverage in all directions. The signal from the patches is combined directly on a PCB splitter.

GNSS Antennas

Two GNSS patch antennas are mounted on opposite sides of the rocket body to provide full-sky coverage at any rotation and improve signal reception. Each antenna signal is amplified by a Low Noise Amplifier (LNA), then combined with a resistive power combiner/splitter. This setup ensures reliable reception across the entire sky.

The GNSS antennas are centered at 1575 MHz for the L1 band and are also right-hand circular polarized. Due to their larger size, only two patches are used, uniformly mounted on the carbon fiber body of the rocket.

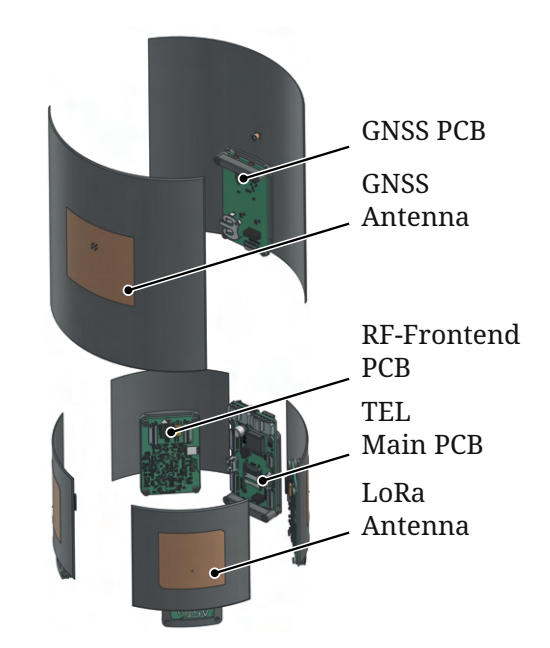


Figure 2.52: Patch antennas are placed on the shell of the avionics section, PCBs directly on the inside.



2.7.2 PCBs

Three different boards are used for the telemetry system in the rocket: the main board, the GNSS board, and the RF-frontends. Boards of the same design are also used in the mission control and the filling station.

The telemetry PCBs inside the main rocket body are mounted on 3d-printed holders directly on the inside of the avionics shell. This is done in order to shorten the signal path to the antennas. In the rocket, the main board is connected to the flight computer and other subsystems via a CAN bus. The GNSS board and RF-frontends are connected to the main board using flat flex cables.

Main board

The telemetry main board is where all parts of the wireless system come together, all controlled by a MCU which then communicates to the rest of the rocket via a CAN bus. Using Flexible Flat Cables the GNSS board, the RF frontends, and the ethernet PCB are also connected to this PCB and form the rest of the telemetry system.

This board also contains the SX1280 LoRa transceiver with matching network and bandpass filter, which generates the RF signals and distributes them to the frontends through either a 4-way splitter or a single output.

Furthermore, a micro SD card slot is integrated into the main board, allowing data to be saved locally.





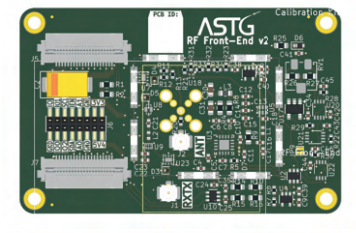
Figure 2.53: Telemetry main board front and back.

RF-Frontend PCB

To improve the link budget and increase the range of the half-duplex telemetry system, a dedicated RF-frontend PCB is implemented to amplify the RF signals. The same antennas are used for both the transmission and reception modes; therefore, the frontend provides a dedicated amplifier for each function. For each mode, the required amplifier is activated and inserted in between the antenna and the transceiver port by means of two absorptive RF-switches SKY13348-374LF.

In reception mode, the LNA path is activated. It features a Transient Voltage Suppressor (TVS) diode and a band-pass filter to protect the input, as well as a BGA9H1BN6 LNA to amplify the signal. This LNA features several modes of operation to activate or bypass the amplifier depending on the received signal strength. For transmission mode, a SE2623L Power Amplifier (PA) is used to boost the signal power up to 27 dBm (500 mW).

As this amplifier puts out higher power, it needs protection against incident reflected power in case of a mismatched antenna. In order to implement protection, two features are added to the amplifier circuit. First, a TVS diode on the output of the amplifier limits the voltage that can be present on this port, protecting the circuit from overvoltage. Secondly, the power reflected from the antenna port is tapped by a cross-coupler and determined by an active detector (MAX2204). If the reflected power exceeds a pre-set value, a latching circuit is activated and disables the PA. The next time the mode is set to reception and back to transmission, the latching circuit is reset and the PA is activated again.



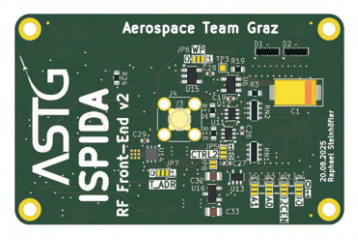


Figure 2.54: Telemetry RF-frontend PCB.



GNSS PCB

In order to accurately and reliably provide GNSS-derived position information on the rocket, a GNSS PCB is added to the telemetry system. This PCB holds two interchangeable GNSS System-On-Modules (SOMs) used to decode the signal of various GNSS systems. The signals received from both antennas are amplified by 19.6 dB using a BGA524N6 LNAs for each antenna. The amplified signals are then combined and split by a resistive combiner/splitter. This is implemented so that each GNSSs' LNA is receiving a signal from both antennas.

To further improve the reliability and availability of GNSS information, a back-up battery on the PCB supplies the SOMs throughout periods where there is no power supplied by the main board (e.g., reboot of the avionics). This enables the SOMs to receive GNSS signals continuously and hold their lock, which otherwise would take up to 1.5 min to establish.



Figure 2.55: GNSS PCB with two separate modules.

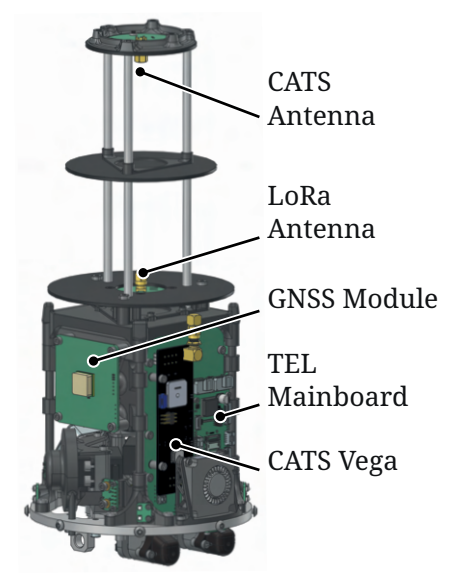


Figure 2.56: Telemetry in the nosecone stack.

2.7.3 Nosecone Telemetry System

The nosecone, as its own landing vehicle, also uses a second instance of the telemetry system as in the main rocket body. The telemetry main board is mounted on the nosecone stack alongside two standalone GNSS PCBs on opposite sides; these are reused from the previous projects AVES II and HALCYON.

Furthermore, there are two identical 2.4 GHz monopole antennas mounted higher up in the nosecone, one is used for the SRAD LoRa link, and the other is for communication with the CATS Vega. A PCB with a matching network is used to electrically tune each antenna to its surroundings.

2.7.4 Firmware

The telemetry firmware uses FreeRTOS as an operating system. It is built in a modular way, allowing the same software components to be used across all nodes: the rocket, the receivers in the mission control, and the ground support equipment at the launch rail.

Both cores of the STM32H745 MCU run their own FreeRTOS instance. The CM4 core is dedicated to LoRa communication, while the CM7 core handles all other tasks, such as CAN communication with rocket subsystems, reading GNSS data over UART, and measuring voltages, currents, and temperatures through the Analog-to-Digital Converter (ADC). Data exchange between the two cores is done through a queue in shared memory, with hardware semaphores ensuring safe access to it. Communication with the radio transceiver is handled over SPI, and all data transfer over UART, ADC, and SPI uses Direct Memory Access (DMA) to reduce processor load.

For data transmission, the system uses LoRa between the rocket and the mission control, CAN bus inside the rocket and GSE, and User Datagram Protocol (UDP) networking between all ground systems. All channels use the custom Teltalk protocol, which standardizes packet transmission, routing, and integrity checks in our system.

2.7.5 Teltalk Communication Protocol

Teltalk regulates how the various MCUs communicate. It encodes the data into an efficient bitlevel-packed representation and implements pings, log messages, commands, a special format for



Technical Report



high-frequency sampled datapoints, throughput/goodput network statistics, packet fragmentation, and integrity checksums.

The C library is generated on the basis of a spreadsheet, which enables rapid development when a new command or sensor is added. To avoid conflicting versions, the command and data packets are guarded with identifiers that are based on the hash of its definition, virtually eliminating the possibility of parsing an incompatible packet.

Teltalk is agnostic about its lower transport layers and does not provide guarantees of reliable or duplicate delivery. Specifically, Ethernet/IPv4/UDP, LoRa, CAN bus are utilized across the whole network.



2.8 Payload Subsystem

ISPIDA is designed to carry a 1U CubeSat. This year marks an exciting milestone as ASTG launches its first international collaboration, carrying a payload from a foreign university team.

2.8.1 Project Description "S2OUTH"

S²OUTH is a modern telemetry system developed by WüSpace e.V., a student team from Würzburg. Its capabilities include redundant sensor data collection and processing, data transfer over >200 km, and live video streaming up to 100 km. The system aims to provide a fully featured, cost-effective telemetry solution for experimental aerospace projects.



2.8.2 System Architecture

The system is built around up to four redundant STM32F405-based computers interconnected by a central CAN bus. The CAN bus connects peripherals including sensors, transmitters, GSE connections, and actuators. A custom-designed redundant power supply provides isolated, stable power to all subsystems.

2.8.3 Telemetry Link

The system uses an adapted open-source OpenLST design for the 70 cm radio band, featuring newer components, a stronger amplifier, and seamless CAN bus integration. It has been tested at distances >250 km with data rates >10 kb/s.



2.8.4 Live Video Stream

HD video transmission up to 100 km is achieved using 5.8 GHz WiFi technology from small IP cameras (<3 cm). The transmission chain uses an RF chip with a power amplifier providing up to 5 W, received by high-gain directional antennas.

2.8.5 Support Systems

The payload receives 24 V and up to 1 A via umbilical at the launch pad. At T-20, ISPIDA's flight computer stops power supply, signaling the payload to transition into launch state.



3 Mission Concept of Operations Overview

3.1 Arming of the System

Integration and Transport: The arming screws are open, mechanically disconnecting all energetic devices from power sources.

At the Launch Rail: After the rocket is mounted on the launch rail in a horizontal position and all umbilicals are connected, the arming screws will be tightened. The igniter circuits are still disconnected from the rocket's flight computers by the arming PCBs.

Before Launch: When the Launch rail officer leaves the launch site, he arms the rocket and nosecone using separate key switches in the safety control box. This sends signals over two redundant electrical connections per arming system, using separate mechanical switches for each cable. This enables the redundant MOSFETs on the arming PCBs, supplying power to the igniter circuits. In addition, a separate key switch arms the engine ignition and holddown circuits.

Launch: When the rocket lifts off, all electrical umbilicals are automatically disconnected from the rocket.

3.2 Tanking and Pressurizing

The tanking procedure involves the following steps:

- Set the vent control to 15 bar
- Open the oxidizer fill valve completely
- Once liquid venting is observed at the upper vent valve, close the oxidizer fill valve
- The system now enters standby mode, awaiting the pressurization and launch GO from EuRoC
- Perform a top-off: reopen the oxidizer fill valve until liquid venting resumes, then close it again
- Vent the oxidizer fill line
- Disconnect the oxidizer QD
- Open the first pressurizing fill valve to pressurize the pressurant tank to approximately 280 bar
- The oxidizer tank is pressurized to 44 bar via the internal COPV and the pressurization system
- Reopen the first N₂ fill valve to bring the pressurant tank to approximately 260 bar
- Open the second N₂ fill valve; the COPV reaches approximately 300 bar
- Vent the N2 fill line
- Disconnect the N₂ QD



3.3 Nominal Flight

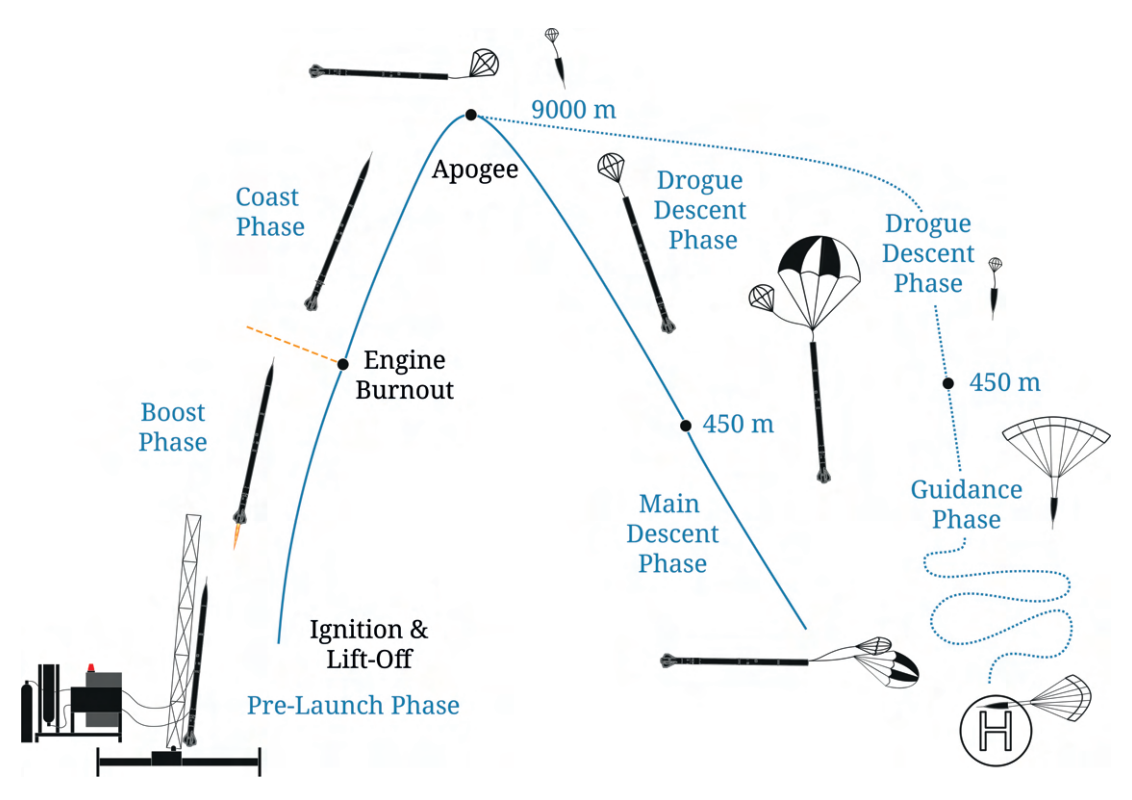


Figure 3.1: Overview of ISPIDA flight cycle showing the complete mission sequence from launch to landing.

3.3.1 Boost Phase

After ignition, the main valve opens and the engine accelerates the rocket off the rail. As it moves upward, the electrical umbilical is automatically disconnected. After 9.5 s, the oxidizer tank is empty. Pure $\rm N_2$ then flows through the engine and extinguishes all flames. The end of acceleration marks the end of the boost phase.

3.3.2 Coast Phase

After engine burnout, the rocket follows its ballistic trajectory. The flight computer calculates the estimated apogee using its Kalman filter and sends signals to the air brake to prevent overshooting the target apogee. When apogee is detected by the flight computer or the CATS Vega, the FD is triggered, ejecting the nosecone and drogue parachute. From this point onward, BUBO follows its independent flight path.

3.3.3 Droque Descent Phase

The main rocket body descends under its drogue parachute with a terminal velocity of (29.0 \pm 1.5) m/s. Meanwhile, BUBO descends with its own drogue parachute, slowing it down to approximately (27.0 \pm 1.5) m/s.



3.3.4 Main Descent Phase

When the main flight computer or the CATS Vega in the main rocket detects an altitude below $450 \, \text{m}$ AGL, it triggers the SD, which releases the main parachute, slowing the main rocket body to a terminal velocity of $(5.7 \pm 1.3) \, \text{m/s}$.

Meanwhile, BUBO also triggers its parafoil deployment and begins its guided sequence. Initially, it flies in a circle to determine wind drift, then navigates toward its designated landing point. At approximately 5 m above ground level, it reduces velocity as much as possible and tilts the nosecone to achieve a safe landing.

3.4 Abort Scenarios

For the launch sequence to be interrupted at any time before lift-off, the order of operations is flipped. To disarm the rocket, the Launch rail officer presses the disarm buttons at the safety control box. This sends a signal over the umbilical cable and disables all MOSFETs, removing power from the igniter circuits. With a possible data link obstruction, the bottom vent valve located inside of the rocket can be manually overridden via the vent valve override key to depressurize the rocket manually. After successful depressurization of the rocket, the electrical connection to the engine ignitor is disconnected, and the ignitor cables are shunted again. Next, the gas bottles are closed, and the filling panel is depressurized and purged via the manual vent valves.

3.5 Thrust Curves

Figure 3.2 shows the thrust curves of all Hot-Fire tests. For the following flight simulations, the thrust curve of HF 6.3 was used, as it is the test closest to the needed total impulse and closely resembles the flight performance.

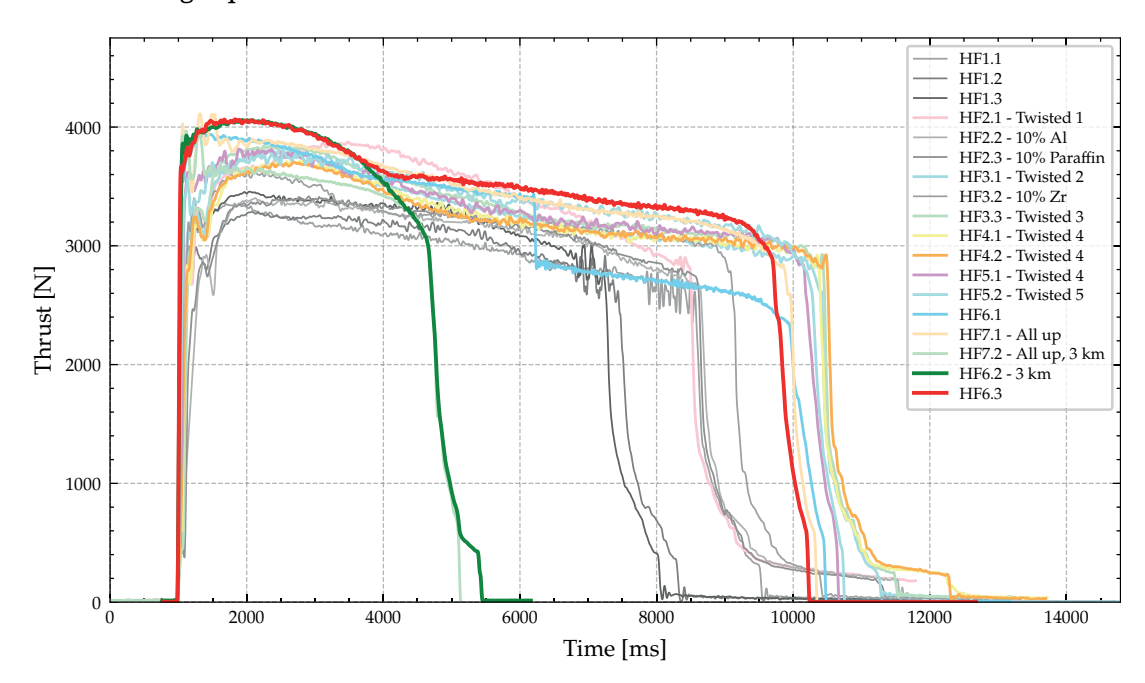


Figure 3.2: Thrust curves of all Hot-Fire tests. The thrust curves were filtered with butterworth filter (order=2, f_crit=20 Hz, python scipy, filtfilt function) for better visibility. The unfiltered thrust curves can be looked up in the corresponding test reports.



3.6 Flight Simulation

Figure 3.3 depicts the trajectory of an ISPIDA flight simulated using rocketpy. Without the air brake and average EuRoC weather conditions, the rocket reaches an apogee of 9523 meters. The used thrustcurve is the one from Hot-Fire test 6.3, as seen in Figure 3.2. The off-the-rail velocity exceeds 30 m/s in every simulated environment, and the stability margin never drops below the stated requirement of 1.5 calibers.

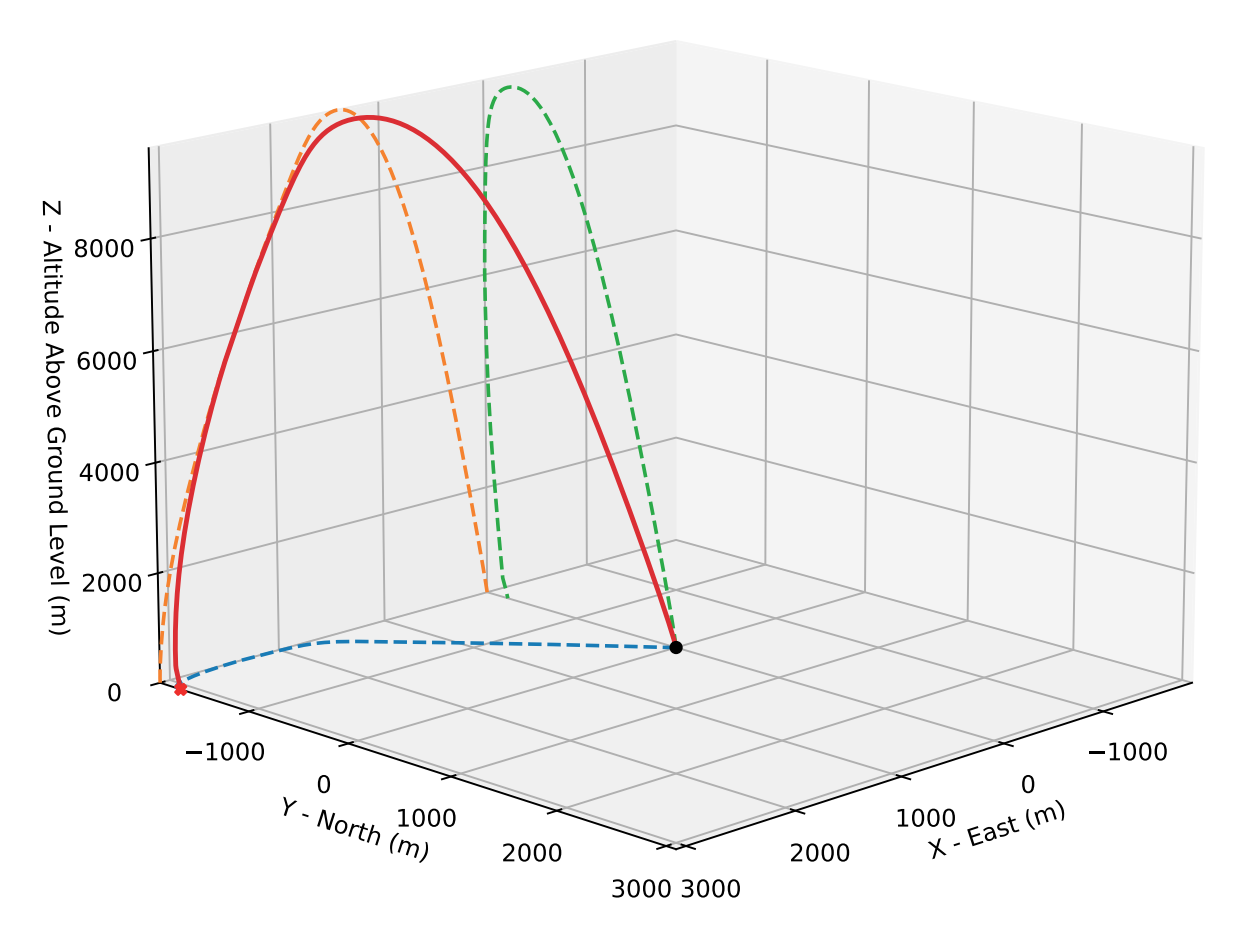


Figure 3.3: Flight trajectory of an ISPIDA flight using the average weather conditions at the EuRoC launch site.

Multiple trajectories for different wind speeds were simulated. The most important parameters are listed in table Table 3.1.

Table 3.1: Apogee, stabilities, and drift distances for different surface windspeeds simulated with rocketpy, not including the air brake.

Wind speed [m/s]	Apogee [m]	Drift [m]	Off-rail stability [cal]	Max stability [cal]
0.0	9414.0	2142.6	3.01	4.65
2.0	9315.1	2191.3	3.01	4.65
4.0	9191.0	2215.0	3.01	4.65
6.0	9040.8	2217.2	3.01	4.65
8.0	8869.6	2197.7	3.01	4.65

Detailed flight simulations can be found in the appendix Chapter H.



4 Conclusions and Outlook

As the third hybrid rocket developed by ASTG, ISPIDA represents the culmination of the team's hybrid propulsion technology to date. Building upon the experiences gained from the last projects, the vehicle integrates design improvements in all major subsystems, enabling higher performance, increased reliability, and a more sophisticated recovery concept.

The main achievements of the project include the successful development and verification of a hybrid propulsion system with active pressurization control, the implementation of a guided recovery nosecone capable of autonomous flight, the integration of a custom-built SRAD flight computer, a Pitot-Static-Probe, as well as an air brake for precise altitude control. These innovations collectively mark a significant step forward compared to earlier ASTG projects.

Reflections on the overall outcome highlight the effectiveness of systematic subsystem testing and incremental design improvements. The structured Hot-Fire campaign provided valuable insights into fuel grain regression behavior, oxidizer mass flow control, and combustion stability, confirming the viability of the chosen grain geometry. Similarly, recovery system testing verified the robustness of dual deployment mechanisms and the functionality of the parafoil guidance system. On the avionics side, the modular CANary approach proved effective for distributed data acquisition and robust communication.

From a project management perspective, lessons were learned in planning, subsystem integration, and documentation. Early prototyping and redundancy in testing reduced risks, while challenges in manufacturing tolerances and supply chain delays emphasized the need for buffer times in future projects. Team collaboration across disciplines proved essential for solving integration issues between propulsion, avionics, and recovery systems.

Looking forward, several areas for improvement remain. The precision of the E-Reg pressurization system can be further refined to improve predictability under varying thermal conditions. Aerodynamic stability and drag reduction can be optimized through additional CFD studies and wind tunnel verification. On the recovery side, further iterations of the parafoil guidance algorithm may enhance accuracy under strong wind conditions. Moreover, future propulsion projects will transition towards liquid propulsion technology as a long-term objective.

Overall, ISPIDA demonstrates the maturity of ASTG's hybrid rocket program. The project not only advances the technical state-of-the-art within the team but also provides valuable knowledge transfer to younger members. The lessons learned form a solid foundation for future developments, as ASTG continues to pursue increasingly ambitious aerospace projects.

List of Figures

1.1	All ASTG rockets	1
1.2	Overview of the team demographics	2
2.1	Overview of ISPIDA	3
2.2	Propulsion stack	4
2.3	Fluid system of the rocket	5
2.4	Upper fluid system cut view	6
2.5	E-Reg controller overview	6
2.6	Upper fluid system	7
2.7	Lower bulkhead	8
2.8	Combustion chamber assembly	9
2.9	Thrust Plate	10
2.10	Cutaway view of the ignitor	10
2.11	Cross section of the fuel grain	11
2.12	Sections of the rocket	13
2.13	Radax connection	14
2.14	Valvebay structure	15
2.15	Assembly of the air brake	16
2.16	Rear view of the fins and the tail section	16
2.17	Pitot-Static System overview	17
2.18	PSP Tube	18
2.19	PSP Stack	18
2.20	Overview of the assembled REC section	19
2.21	Chargecup with ignitors molded in PU	20
2.22	Sectional view first deployment	20
2.23	Explosion view of first deployment	20
2.24	Assembled 3D and sectional view of the SD	21
2.25	Drogue parachute descent with SPATZ test rocket	22
2.26	Drogue parachute and main parachute parachutes	23
2.27	Main parachute bag	23
2.28	Rotatable swivel	24
2.29	Line reinforcement	24
2.30	Softshackle	24
2.31	Breakdown of the nosecone insert	25
2.32	Exploded view of the steering mechanism	25
2.33	3D and sectional view of the Parafoil deployment	26

2.34	Nosecone PCBs	26
2.35	Parafoil in flight with the teststand	28
2.36	Rocket PCBs	29
2.37	Power distribution overview	30
2.38	Battery pack	30
2.39	Avionics stack	31
2.40	Main flight computer	32
2.41	Sensor Board	32
2.42	Black Box	32
2.43	Backplane	33
2.44	Arming PCB	33
2.45	REC Interface	33
2.46	CANary PCB	34
2.47	Sun Sensor PCB	34
2.48	Recovery system cross redundancy	35
2.49	State diagrams	36
2.50	Launch sequence states	37
2.51	Automatic state detection	37
2.52	Patch antennas	39
2.53	Telemetry main board	40
2.54	Telemetry RF-frontend PCB	40
2.55	GNSS PCB	41
2.56	Telemetry in the nosecone stack	41
3.1	ISPIDA Flight Cycle	45
3.2	Thrust curves of all Hot-Fires	46
3 3	Trajectory of the flight simulation	47

List of Tables

2.1	Engine characteristics	4
2.2	Summary of the Hot-Fire campaign	12
2.3	Properties of the wound REC shell	14
3.1	Flight simulation results	47

Acronyms

Ar Argon.

ABS Acrylonitrile Butadiene Styrene.

ADC Analog-to-Digital Converter.

AGL Above Ground Level.

AHRS Attitude Heading Reference System.

APEX Auroral Polarization EXplorer.

ARB Axial Ratio Bandwidth.

ASA Acrylonitrile Styrene Acrylate.

AST Aerostructure Module.

AVI Avionics.

CAN Controller Area Network.

CATS Control and Telemetry Systems.

CFD Computational Fluid Dynamics.

CFRP Carbon-fiber Reinforced Polymer.

COPV Composite overwrapped pressure vessel.

COTS Commercial-off-the-shelf.

DMA Direct Memory Access.

DuT Device under Test.

EuRoC European Rocketry Challenge.

FD first deployment.

FEA Finite Element Analysis.

FEP Fluorinated Ethylene Propylene.

FFG Austrian Research Promotion Agency.

FLI Flight Computer Module.

FMECA Failure Mode, Effects and Criticality Analysis.

FS Filling Station.

GFRP Glass-fiber Reinforced Polymer.

GNSS Global Navigation Satellite System.

GSE Ground Support Equipment.

HTPB Hydroxyl Terminated Polybutadiene.

I/O Input/Output.

IFT Institute of Production Engineering.

IIM Institute of Innovation and Industrial Management.

IMAT Institute for Material Science, Joining and Forming.

IMU Inertial Measurement Unit.

IPDI Isophorone Diisocyanate.

LED Light Emitting Diode.

LHCP Left-Hand Circular Polarized.

Li-ion Lithium-ion.

LNA Low Noise Amplifier.

MCU Microcontroller Unit.

MGC Main Guidance Computer.

NACA U.S. National Advisory Committee for Aeronautics.

NASA National Aeronautics and Space Administration.

PA Power Amplifier.

PCB Printed Circuit Board.

PCIe Peripheral Component Interconnect Express.

PD Parafoil deployment.

PID Proportional Integral Differential.

PoE Power over Ethernet.

PRO Propulsion Module.

PSD photosensitive diode.

PSP Pitot-Static-Probe.

PTFE Polytetrafluoroethylene.

PU Polyurethane.

PWM Pulse-width Modulation.

QD Quick Disconnect.

QFH Quadrifilar Helix.

RC Radio Controlled.

REC Recovery Module.

REXUS Rocket Experiment for University Students.

RF Radio Frequency.

RHCP Right-Hand Circular Polarized.

RSSI Received Signal Strength Indicator.

RTA Rail Tec Arsenal.

RTOS Real-time Operating System.

SD second deployment.

SF Safety Factor.

SLS Selective Laser Sintering.

SNR Signal-to-noise ratio.

SOM System-On-Module.

SPI Serial Peripheral Interface.

SRAD Student Researched and Developed.

TEL Telemetry Module.

TPU Thermoplastic Polyurethane.

TU Graz Graz University of Technology.

TVS Transient Voltage Suppressor.

UART Universal Asynchronous Receiver Transmitter.

UDP User Datagram Protocol.

UPS Uninterruptible Power Supply.

USB Universal Serial Bus.

WLAN Wireless Local Area Network.

Glossary

3d-printed Manufacuring method, typically joining adding material together layer by layer.

air brake A deployable aerodynamic surface used to increase drag and slow down the rocket during ascent.

airframe The mechanical structure of a rocket or airplane.

ALCEDO 9 km Hybrid rocket designed by the Aerospace Team Graz 2023/24 for the European Rocketry Challenge.

ASTG Aerospace Team Graz founded in Oct. 2019.

AVES II $\,$ 3 km solid rocket designed by the Aerospace Team Graz 2021/22 for the European Rocketry Challenge.

avionics mount System that holds all the control electronics within the rocket.

avionics stack They fully assembled avionics system, i.e. the avionics mount equipped with all PCBs.

backplane PCB that serves as an interconnection between slot-in PCBs.

blackbox Hardened data storage device designed to survive ballistic impacts.

BUBO Landing vehicle consisting of the nosecone of ISPIDA that uses a parafoil to glide to a predefined landing spot.

CANary Control and data acquisition module connected via CAN bus.

CATS Vega COTS altimeter and recovery electronics from CATS.

Cold-Flow Rocket engine test without ignition.

coupling tube Tube for separable connection between nose cone and recovery shell.

CubeSat Miniaturized satellite with form factor of a 100 mm cube.

drogue parachute A small parachute deployed at apogee, to stabilize the vehicle's altitude, and reduce its descent rate sufficiently to permit the main deployment event, yet not so much as to exacerbate wind drift.

E-Reg Active pressure control system, consisting of a servo controlled ball valve.

Flexible Flat Cable A type of electrical cable that is both flat and flexible, with flat solid conductors

Flexible Printed Circuit Board A type of PCB designed to be bent, folded or twisted.

flight computer Onboard system that manages the control, and data processing functions of the vehicle during flight.

Flip-Flop A digital circuit element that can store one bit of binary information and has two stable states. It acts as a basic memory unit that can be switched between its two states (typically representing logic 0 and 1) by input signals. Flip-flops are fundamental building blocks in sequential logic circuits and are commonly used for data storage, state control, and signal latching in digital systems.

FreeRTOS Real-time operating system for embedded devices.

HALCYON 3 km hybrid rocket designed by the Aerospace Team Graz 2022/23 for the European Rocketry Challenge.

Hot-Fire Rocket Engine Test with Combustion in the Combustion Chamber.

ignitor Axial engine ignitor in C-shape designed to ignite the port of the fuel grain.

ISM band Radio spectrum reserved internationally for industrial, scientific, and medical purposes.

ISP Specific Impulse; a measure of the efficiency of a rocket engine, usually expressed in seconds.

ISPIDA 9 km Hybrid rocket designed by the Aerospace Team Graz 2024/25 for the European Rocketry Challenge.

Launch rail officer Person responsible for operations at launchpad.

LoRa Radio communication technique.

main flight computer Main flight computer PCB with the MCU that controls the rocket as well as the filling station.

main parachute A second, large parachute deployed no higher than 450 m AGL, reduce the vehicle's descent rate sufficiently to prevent excessive damage upon impact with the ground.

main valve The valve connecting the oxidizer tank to the combustion chamber.

mission control Facility to manage launch and test operations.

mission control officer Person in charge of the mission control.

MOSFET Metal-Oxide-Semiconductor Field-Effect Transistor. A type of field-effect transistor that is commonly used for switching and amplifying electronic signals. MOSFETs are voltage-controlled devices that can handle high currents and voltages with low power consumption, making them ideal for power management applications in electronic circuits.

nosecone Cone-shaped front part of the rocket.

O/F ratio Oxidizer-to-Fuel ratio; describes the mass ratio of oxidizer to fuel in a propellant mixture.

parafoil A steerable, non-rigid, rectangular airfoil connected to the vehicle via two steering lines. As a replacement for a main parachute, it stabilizes the vehicle's altitude, and reduce its descent rate.

PID controller Feedback control system with proportional, integral, and derivative terms to minimize control error.

pyrotechnic mass Mixture used in the engine ignitor consisting of 60% rocket candy, 25% calcium silicide (CaSi) and 15% magnesium powder.

Radax Radial-axial, a type of airframe joint, describing the angled contact surface and force transfer.

ram-air parachute Ram-air parachutes are a type of parafoil parachute designed to reduce descent speed and ensure a safe landing. Their main advantage lies in the high level of control they provide over both direction and speed, while also generating lift through their aerodynamic design. Constructed from two layers of ripstop nylon, they feature cell-like airfoil chambers that inflate with air during flight, giving the canopy its shape and stability.

RavenOS Self-developed RTOS running on the main FLIGHT COMPUTER.

SPATZ test rocket SRAD modular low-cost test rocket developed for flights around 100 m AGL.

STM32 Family of 32-bit microcontroller integrated circuits based on the ARM Cortex-M cores, manufactured by STMicroelectronics.

tailcone Cone-shaped cover at the rear of the rocket.

Teltalk Custom data transfer protocol.

References

- [1] Colin D. Hill, Will Nelson, and Craig T. Johansen. "Evaluation of a Paraffin/Nitrous Oxide Hybrid Rocket Motor with a Passive Mixing Device." In: *Journal of Propulsion and Power* 38.6 (Nov. 2022), pp. 884–892. ISSN: 1533-3876. DOI: 10.2514/1.B38659.
- [2] Tobias Peter Scheipel et al. "SmartOS: An OS Architecture for Sustainable Embedded Systems." In: *Fruehjahrstreffen FG BS*. Gesellschaft für Informatik, Mar. 2022.



Appendix A: System Data

Table A.1: System Data - Outer Dimensions and Mass Distribution.

Total Length	4357 mm
Length of main body (without PSP)	4189 mm
Diameter	152.4 mm
Total Mass (dry / wet)	29.4 kg / 47.0 kg
Mass Airframe Tailcone	1600 g
Mass Combustion Chamber	4500 g
Mass Air Brake	1100 g
Mass Fluid System	10 400 g
Mass Airframe Avionics Section	1500 g
Mass Avionics Stack	900 g
Mass Airframe Recovery Section	1250 g
Mass Recovery Subsystem	4400 g
Mass Airframe Nosecone	550 g
Mass Guided Nosecone	2000 g
Mass Payload	1000 g
Mass Official Flight Tracking (CATS	200 g
Vega) incl. Mounting	
Mass Fuel (HTPB)	2500 g
Mass Pressurizing Gas (N ₂)	1600 g
Mass Oxidizer (N ₂ O)	13 500 g

Table A.2: System Data - Flight Data.

Target Apogee	9000 m
Velocity off Rail	40 m/s
Max. Velocity	521 m/s
Max. Acceleration	90 m/s ²
Time to Apogee	48 s
Total Flight Time	244 s

Table A.3: System Data - Aerostructure.

Drag Coefficient	0.24 to 0.63
Dry Center of Gravity (reference: tip)	2714 mm
Moment of Inertia (long axis)	$0.07\mathrm{kgm^2}$
Moment of Inertia (short axis)	34.59 kgm ²
Fin Geometry	Trapezoidal

Table A.4: System Data - Recovery.

First Deployment Event	Apogee (9000 m AGL)
Main Deployment Event	450 m AGL
Descent Velocity Drogue Parachute	(29.0 ± 1.5) m/s
Descent Velocity Main Parachute	$(5.7 \pm 1.3) \mathrm{m/s}$
Panel side length Drogue Parachute	0.5 m
Diameter Main Parachute	3.0 m
Opening Shock Drogue	(5013 ± 180) N at 200 m/s
Opening Shock Main	939 N at 75 m/s



Table A.5: System Data - Guided Nosecone.

Separation Event	Apogee (9000 m AGL)
Parafoil Deployment Event	450 m AGL
Descent Velocity Drogue Parachute	(27.0 ± 1.5) m/s
Descent Velocity Main Parachute	5 m/s to 5.5 m/s
Panel side length Drogue Parachute	10 cm
Span of the parafoil	1.65 m
Glide ratio (straight flight)	2.5:1 (horizontal:vertical)
Glide ratio (truing turns)	1.4:1 (horizontal:vertical)

Table A.6: System Data - Flight Computer.

SRAD Standby Time with Umbilical	> 24 h
Connection	
COTS Standby Time	8h-10h
SRAD Standby Time without Umbili-	3h-4h
cal Connection	
Barometer Sampling Frequency	60 Hz
Processor Frequency	480 MHz
Data Storages	2
Quantity Sensors (complete rocket	76
without COTS)	
Quantity PCBs (complete rocket,	85
without COTS, including nosecone)	
Quantity Cameras (excluding Pay-	6
load)	

Table A.7: System Data - Telemetry.

#1 System Type	LoRa (Rocket)
#1 Frequency Range	2400 to 2500 MHz
#1 Bandwidth	1.6 MHz
#1 RF Power	Up to 1.5 W
#1 Data Uplink	Configuration Parameters & Com-
	mands
#1 Data Downlink	Rocket Data & Position
#1 Range	> 30 km
#2 System Type	LoRa (Nosecone)
#2 Frequency Range	2400 to 2500 MHz
#2 Bandwidth	1.6 MHz
#2 RF Power	Up to 1.5 W
#2 Data Uplink	Configuration Parameters & Com-
	mands
#2 Data Downlink	Nosecone Data & Position
#2 Range	> 30 km



Table A.8: System Data - Propulsion.

Engine	SRAD Hybrid
Fuel	HTPB
Fuel Mass	2500 g
Oxidizer	Nitrous Oxide N ₂ O
Oxidizer Mass	13 500 g
Pressurizing Gas	Nitrogen N ₂
Pressurizing Gas Mass	1600 g
Total Impulse	32.1 kN · s
Max. Thrust	4000 N
Burn Time	9.5 s
Combustion Chamber Pressure	30 bar
Dry Mass	14 900 g
Length	2690 mm
Ignition Type	Pyro

Table A.9: System Data - Payload.

Form Factor	1x CubeSat 100 x 100 x 113.5 mm
Mass	1000 g
Quantity Payloads	1

Table A.10: Summary of SF of most critical parts in the Aerostructure Subsystem. Given are functional groups (eg. Radax: adhesive joint, screws, Radax female and male), and the lowest SF of that working group is given.

Group	SF	Point of First Failure	Reference	
12-point-RADAX	3.33	M4 RADAX Screws	Calc Chapter K	
6-point-RADAX	2.12	M5 RADAX Screws	Calc Chapter K	
Air Brake	3.29	M8 Connection Screws	Calc Chapter K	
Shell	1.5	AVI shell	Tube bending test Chapter K	
Fins	2.15	Foot of Fin	FinSim	

Table A.11: Summary of SF of most critical parts in the Recovery Subsystem. Given are components, the SF and the reference document.

	SF		
Component	Nominal at 100 m/s	Reference	
_	[unlikely at 200 m/s]		
Drogue parachute Shroud Line	43.37 [9.14]	Tension scale test Appendix C.4	
Rotatable Carabiner	21.64 [4.59]	Datasheet Section L.3.1	
Softshackle	18.815 [3.98]	Tension scale test Appendix C.5	
Pressure Plate Bolt	>9.45 [>1.91]	FEA Chapter K	
40 mm Lash on Bag	23.52 [4.98]	Datasheet Section L.3.1	
3 mm Line	5.86 [1.23]	Tension scale test Appendix C.4	
4 mm Line	7.07 [1.49]	Tension scale test Appendix C.4	
8 mm Lines	11.97 [2.52]	Datasheet Section L.3.1	
Eyebolt	46.57 on SD shock	Datasheet Section L.3.1	
SD	14.71 [3.32]	FEA Chapter K	
Groundplate	6.95 [1.75]	FEA Chapter K	







Table A.12: Summary of SF of most critical parts in the Propulsion Subsystem. Given are components, the SF and the reference document. The load cases are assumed to be twice the maximum expected pressures (oxidizer tank $56\,\mathrm{bar}$, combustion chamber $30\,\mathrm{bar}$, pressurant tank $300\,\mathrm{bar}$).

Component	2x Maximum pressure	SF	Reference
Bulkhead	112 bar / 60 bar	1.85	FEA Chapter K
Feedpipe	112 bar	4.17	FEA Chapter K
Injectorcover	112 bar / 60 bar	2.27	
Pt-Connector	600 bar	1.03	FEA Chapter K
E-Reg Body	112 bar	1.09	FEA Chapter K
Combustion Chamber	60 bar	1.61	FEA Chapter K
Oxidizer Tank	112 bar	1.01	FEA Chapter K